THESIS

INITIAL DEVELOPMENT OF A MULTISTAGE CANCER MODEL BASED ON SYRIAN HAMSTER EMBRYO (SHE) CELL TRANSFORMATION STUDIES

Submitted by

Kai-hsin Liao

Department of Chemical and Bioresource Engineering

in partial fulfillment of the requirements

for the Degree of Master of Science

Colorado State University

Fort Collins, Colorado

Fall 1999

COLORADO STATE UNIVERSITY

November 5, 1999

WE HEREBY RECOMMEND THAT THE THESIS PREPARED UNDER OUR SUPERVISION BY KAI-HSIN LIAO ENTITLED INITIAL DEVELOPMENT OF A MULTISTAGE CANCER MODEL BASED ON SYRIAN HAMSTER EMBRYO (SHE) CELL TRANSFORMATION STUDIES BE ACCEPTED AS FULFILLING IN PART REQUIREMENTS FOR THE DEGREE OF MASTER OF SCIENCE.

Committee on Graduate Work

[redacted]

Co-Adviser

[redacted]

Adviser

[redacted]

Department Head

ABSTRACT OF THESIS

INITIAL DEVELOPMENT OF A MULTISTAGE CANCER MODEL BASED ON SYRIAN HAMSTER EMBRYO (SHE) CELL TRANSFORMATION STUDIES

To better incorporate biologic information into quantitative cancer modeling, the two-stage MVK (Moolgavkar-Venzon-Knudson) model has been modified for use with SHE cell neoplastic progression. Conceptually, five phenotypic stages are included in this model: normal cells can either become senescent or mutate into immortal cells followed by anchorage-independent growth and tumorigenic stages. Cells in each stage have distinct division, death and mutation rates, and mutation is assumed to occur during cell division. Model development and related experiments were focused on studying the abilities of lead, arsenic, chromium, and a mixture of these three metals to induce progression of SHE cells from one phenotype to the next. Cell division and death rates were assessed using flow cytometric analysis for inclusion in the model. Cell division rates were measured using bromodeoxyuridine (BrdU) incorporation with propidium iodide staining, which allows for the calculation of potential doubling time, a measure of cell cycle time that takes growth

fraction, but not cell loss, into account. Potential doubling times of normal SHE cells ranged from 12 to 59 hours, depending on the degree of confluence of cell cultures. Cell death was measured by a flow cytometry method based on propidium iodide staining specifically related to membrane damage. The mean cell death rate is approximately equal to 1% of the average value of division rates. The individual metals and their mixture did not induce immortalization or further mutations of SHE cells in our laboratory following a 2-day exposure. However, the growth of SHE cells was inhibited by 5.4 μM of arsenic, with cells becoming senescent after only 16 population doublings; whereas, normal cells and cells exposed to lower arsenic concentrations lasted for at least 30 population doublings. The model developed in our laboratory successfully predicted the growth of normal cells. The cell senescence rates under the impact of arsenic exposure were also calculated. Mechanisms responsible for induction of cellular senescence in SHE cells exposed to arsenic may be involved in the apparent inability of arsenic to induce neoplasia in experimental animals.

Kai-hsin Liao
Department of Chemical and Bioresourece Engineering
Colorado State University
Fort Collins, CO 80523
Fall 1999

ACKNOWLEDGMENTS

This work was supported by ATSDR (Cooperative Agreement U61/ATU 881475) and NIEHS Superfund Basic Research Program (P42 ES05949). Dr. Raymond Yang inspired me to have the ideal to innovate the model and provided all the support for this research. Dr. Ken Reardon gave me great guidance in applying my engineering problem-solving skills to a biological system. Dr. Dan Gustafson helped me develop the experimental methods based on model assumptions. Dr. Michael Fox was a wonderful consultant for flow cytometric analysis. Laura Chubb provided great assistance with the tedious experimental processes.

It is joyful to work with the CETT research team members. Thanks to Wendy, Ivan, and Damon for providing mental support. I cherish the friendship, especially as a foreign student. Thanks also to the many other lab members who frequently helped in various aspects of this project.

I would like to give my deepest appreciation to my dearest Wan Chen, who knows me the best and helped me through all the frustrations I had in these years. Helping me count cells, even in Christmas day, was just a small part of that. Thank you.

TABLE OF CONTENTS

CHAPTER 1

Introduction

1.1 Purpose of the project

To further incorporate biologic information into quantitative cancer modeling, the two-stage MVK model (Moolgavkar-Venzon-Knudson; refer to Section 2.2.b; Moolgavkar *et al.*, 1988; Dewanji *et al.*, 1989) has been modified for use with Syrian hamster embryo (SHE) cell neoplastic progression. *In vitro* cell culture offers the advantage that cells from different stages of the transformation process can be isolated for detailed studies. Therefore, it is ideal to measure the parameters needed for biologically-based dose-response modeling from *in vitro* studies.

Model development and related experiments were focused on studying the abilities of lead (Pb^{2+}), arsenic (As^{3+}), chromium (Cr^{3+} + Cr^{6+}; 1:1 ratio), and a mixture of these three metals to induce progression of SHE cells from one phenotype to the next. Laboratory measurements of metal- and metal mixture-induced changes in key cell parameters were used to verify the development of this modified multi-stage carcinogenesis model.

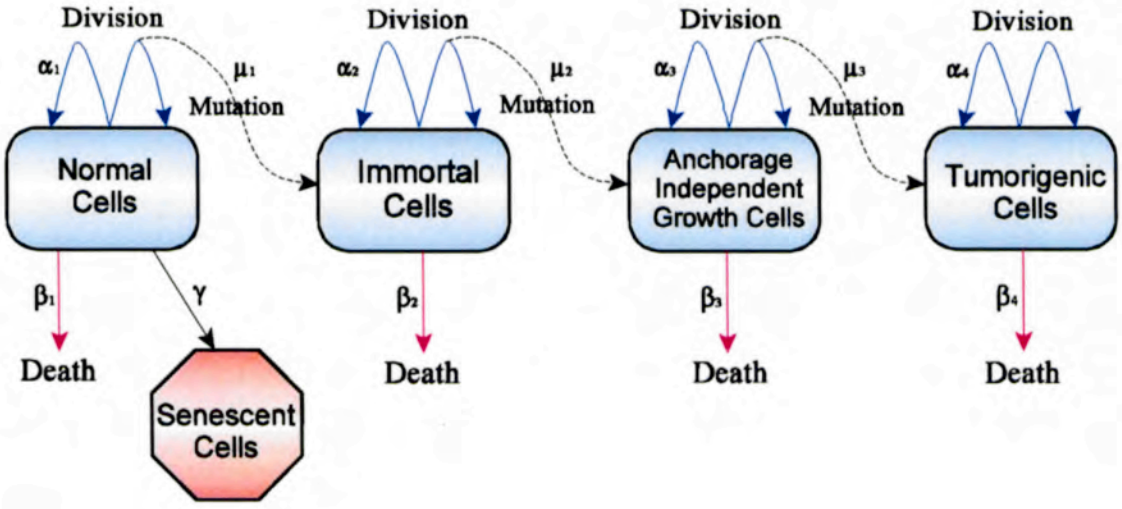

Figure 1.1 Modified multistage carcinogenesis model for SHE cell neoplastic progression

Five phenotypic stages are included in this model: normal, senescent, immortal, anchorage-independent growth, and tumorigenic. Cells in each stage have distinct division, death, and mutation rates, and mutation is assumed to occur only during cell division. α_i and β_i are the cell division and death rates, respectively for cells in stage i. γ is the rate of senescence of normal cells. μ_i is the probability of mutation that a stage i cell divides into one stage i cell and one stage i + 1 cell.

1.2 Modified multistage model of SHE cell neoplastic progression

SHE cells have been used to study neoplastic progression for many years, and, as a result, the phenotypic changes exhibited by the cells during the carcinogenic process are well defined. Two important advantages of the SHE cell system are that the cells exhibit a low frequency of spontaneous transformation and that they readily demonstrate neoplastic transformation upon treatment with chemical carcinogens (Barrett, 1993).

The two-stage clonal growth model that I have chosen to use for the cancer modeling purposes in SHE cells incorporates cell division, death, and mutation rates into the mechanistic description of malignant transformation (Conolly and Kimbell, 1994). Cell division and death determine the population growth within each stage. It is further assumed that mutation only occurs at cell division.

The modified multistage carcinogenesis model for SHE cell neoplastic progression is shown in Figure 1.1. Normal cells in culture cease proliferation after a limited number of cell divisions, a process called cellular senescence. Escaping from senescence to become immortalized is the first important step during carcinogenesis in SHE cells and in many other cell types. Chemical carcinogens will, at some frequency, induce mutations in normal SHE cells that allow them an unlimited life span in culture. As stated above, these mutations are assumed to occur only during cell division.

Immortalized cells are easily detected over the background of normal cells by continued passage in culture. Over time, normal cells cease proliferating and die, while the immortalized clones will gradually take over the culture. However, some chemical carcinogens may inhibit the growth of SHE cells and shorten their life span instead of inducing immortalization.

Upon continued treatment with carcinogens, immortalized SHE cells will subsequently acquire additional mutations, some of which will confer the next important phenotype, that is, anchorage-independent growth. There is a strong positive correlation in SHE cells between anchorage-independent growth and tumorigenicity (LeBoeuf *et al.*, 1990). Anchorage-independent growth can be readily detected by plating the cells in semi-solid media such as methylcellulose or soft agar. Colony-forming efficiency under these conditions is indicative of a cell's transformed nature. Finally, anchorage-independent cells may undergo further genetic alterations that confer the tumorigenic phenotype, *i.e.* the ability to grow tumors in immuno-compromised mice or newborn hamsters.

In this thesis, I have focused on the first stage (normal cells) and the two stages connected to it, immortal and senescent cells. However, it is important to note that all the experimental methods developed in our laboratory so far can be applied to all of the stages of the carcinogenic process in SHE cells. If the model developed through these initial studies

appears to be consistent with experimental data for the first two stages, the same principles and experimental techniques can be easily applied to the subsequent two phenotypic stages.

Based on the conceptual model presented above, equations can be written to describe the time-dependent changes in the populations of normal, immortal, and senescent cells. It is assumed that the rate of change in the number of normal cells, dN(t)/dt, is proportional to the number of normal cells at any time:

$$\frac{dN(t)}{dt} = N(t)\cdot[\alpha_1(t) - \beta_1(t)] - \gamma(t)\cdot N(t) \qquad (1.1)$$

In Equation 1.1, α_1 and β_1 represent the specific rate of cell division and death (units of 1/time) for normal cells; whereas, γ is the rate at which normal cells convert to senescent cells.

Similarly, the rate of change in the immortal cells, dI(t)/dt, has the same exponential growth property (with α_2 and β_2 being the specific rate of cell division and death, respectively), but there is also input of mutated normal cells:

$$\frac{dI(t)}{dt} = I(t)\cdot[\alpha_2(t) - \beta_2(t)] + \mu_1(t)\cdot\alpha_1(t)\cdot N(t) \qquad (1.2)$$

In Equation 1.2, μ_1 represents the probability of mutation that a normal cell

divides into one normal cell and one immortal cell. Since μ is a probability based on the number of cell divisions, it should be multiplied by division rate, α, and the number of normal cells.

The rate of change in senescent cells, dS(t)/dt, is proportional to the cell senescence rate, γ, and the number of normal cells (Equation 1.3) because all senescent cells are converted from normal cells.

$$\frac{dS(t)}{dt} = \gamma(t) \cdot N(t) \qquad (1.3)$$

The growth of cells in anchorage independent growth and tumorigenic stages will be predicted by the computer simulation method proposed by Conolly and Kimbell (refer to Section 2.2.b; Conolly and Kimbell, 1994). The cell growth will be treated stochastically for cells with smaller populations and assumed to be deterministic for cells with larger populations.

As mentioned above, arsenic, lead, chromium, and the mixture of these three metals were examined for their effect on the progression of SHE cells from one phenotype to the next. Cell division and death rates were assessed using flow cytometric analysis for inclusion in the model. Mutation rates could be measured by fluctuation analysis. Details of the methods are discussed in Chapter 3.

CHAPTER 2

Literature Review

2.1 Carcinogenesis

Cancer is a disease caused by uncontrolled cell proliferation. The growth of 50 trillion individual cells, which compose the healthy human body, are carefully controlled to meet the whole body's needs (Cooper, 1992a). Cancer begins when cells become oblivious to the factors that control the proliferation of normal cells and continue to proliferate when they should not. Cancerous cells are capable of invading nearby tissues from the site where they began and become lethal when the tissues and organs needed for the survival of the whole body are disrupted (Weinberg, 1996).

Two gene classes play major roles in the formation of cancer. They regulate the life cycle of the cell through cell growth and division. Proto-oncogenes motivate cell growth, while tumor suppressor genes inhibit cell growth (Weinberg, 1996). Proto-oncogenes can become oncogenes through mutation, which results in unending proliferation of cells. Nevertheless, tumor suppressor genes are inactivated by mutations that allow cells to ignore braking signals and divide excessively (Weinberg, 1996). It is believed

that mutation in at least 6 or more growth-control genes must take place for the development of a cancerous tumor (Weinberg, 1996).

There is strong evidence from human epidemiologic studies and animal experiments that the induction of cancer occurs in more than one stage (Moolgavkar and Knudson, Jr., 1981). Based on *in vivo* experiments, the stages of carcinogenesis were historically defined as initiation, promotion, and progression (Boyd and Barrett, 1990). Initiation results from an irreversible genetic alteration, while promotion is defined as the clonal expansion of initiated cells to a preneoplastic focus or benign tumor. Progression is considered as the conversion of a preneoplastic focus or benign tumor to a malignant tumor (Boyd and Barrett, 1990).

Carcinogens can increase the incidence of cancer in two general ways. Initiating agents, or initiators, induce genetic alterations that result in uncontrolled cell proliferation (Cooper, 1992b). This group of carcinogens includes numerous chemicals and radiation. Other carcinogens, called promoting agents or promoters, stimulate cell proliferation instead of inducing mutation. Promoters are only effective in inducing tumors when initiation stages have been developed (Cooper, 1992b). Examples of promoters include hormones and cigarette smoking (Moolgavkar, 1983).

2.2. Models for carcinogenesis

This section begins with the discussion of the development of cancer models, followed by a review of the MVK (Moolgavkar-Venzon-Knudson) two-stage model which formed the basis of the model developed in this thesis.

2.2.a Development of cancer models

The multistage theory of cancer-inducing mechanism, which assumes a cancer cell is the end-result of a series of discrete mutations, was proposed by Nordling (Nordling, 1953). Motivated by the theory, Armitage and Doll derived a quantitative multistage model (Armitage-Doll multistage model), which relates the logarithm of incidence rate linearly to the logarithm of age, and describes the incidence rate as directly proportional to the dose of an applied carcinogen (Armitage and Doll, 1954). The linearized multistage model (Nordling, 1953; Crump, 1996), a generalization of the Armitage-Doll multistage model, is the default model for carcinogen risk assessment used by Environmental Protection Agency (EPA; Crump, 1996). In the approach used by EPA, cancer risks are estimated from a conservative procedure for low-dose extrapolation calculated from the data of 2-year animal experiments (Portier and Edler, 1990). The linearized multistage model and Armitage-Doll multistage model are statistical dose-response models rather than biological

models, since actual physiological phenomena, *e.g.* cell proliferation, are ignored in the models.

To incorporate the kinetics of cell division and death into cancer model, Armitage and Doll proposed a two-stage model (Armitage and Doll, 1957), the Armitage-Doll two-stage model, which assumes deterministic exponential growth for normal and intermediate cells. The stochastic nature of the growth of intermediate cells were then introduced to the two-stage model by Moolgavkar and colleagues (the MVK model; Moolgavkar, 1979; Moolgavkar and Knudson, Jr., 1981; Moolgavkar, Dewanji, and Venzon, 1988).

2.2.b The MVK two-stage model for carcinogenesis

The MVK two-stage model for carcinogenesis (Moolgavkar, 1979; Moolgavkar and Knudson, Jr., 1981; Moolgavkar, Dewanji, and Venzon, 1988) has been recommended as the major model for the risk assessment of environmental agents in recent years (Tan, 1991). The advantages of this model are that it involves genetic changes and cell proliferation, which are believed to be crucial factors in the carcinogenesis process, while remaining simple enough to be applicable to human incidence data (Tan, 1991). The applications of the MVK two-stage model include the evaluation of risk factors of female breast cancer (Moolgavkar *et al.*, 1980) and the successful

fitting of the incidence functions of all human cancers (Moolgavkar and Knudson, Jr., 1981).

The MVK two-stage model incorporates two features: a) transition of normal cells to cancer cells via an intermediate stage, as the result of two discrete, heritable, and irreversible events, and b) growth and death of normal and intermediate cells (Figure 2.1; Moolgavkar and Knudson, Jr., 1981). The growth of the normal tissue is assumed to be deterministic since numerous normal cells are expected to exist at any time. However, the growth of intermediate cells is treated stochastically because the transition of intermediate cells from normal cells is a rare event. In a small time interval, Δt, a normal cell may divide into two daughter normal cells with probability $\alpha_1 \Delta t$ or it may die (or differentiate) with probability $\beta_1 \Delta t$. It may also divide, with a small probability ($\mu_1 \Delta t$), into one normal cell and one intermediate cell which has suffered the first event. During Δt, an intermediate cell may in turn divide into two daughter intermediate cells, die (or differentiate), or divide into one intermediate and one malignant cell, with probabilities of $\alpha_2 \Delta t$, $\beta_2 \Delta t$, or $\mu_2 \Delta t$, respectively (Moolgavkar and Knudson, Jr., 1981). With the subscripts to distinguish cells in different stages, α, β, and μ are the birth, death, and transition rates per cell per year. It is assumed, in the MVK model, that the number of intermediate cells mutated from normal cells by time t is a random variable, which has a Poisson

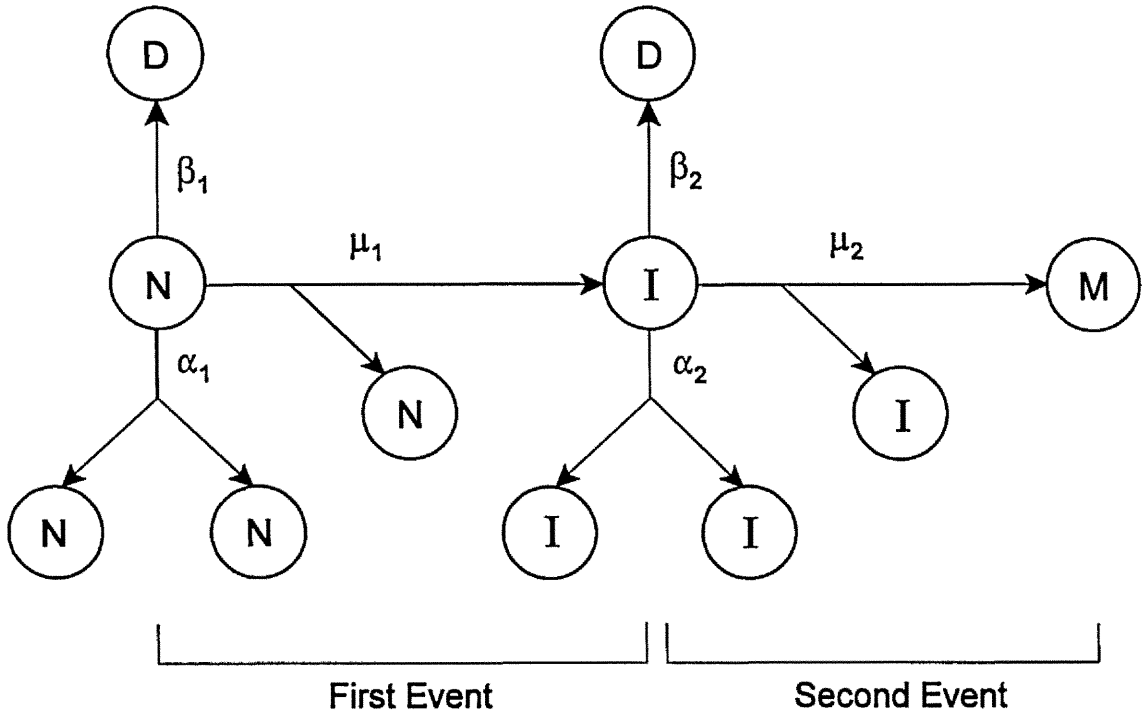

Figure 2.1. Two-stage MVK model for carcinogenesis

N, normal cells; I, intermediate cell; D, dead or differentiated cell; M, malignant cells. α_1, birth rate (per cell per year) of normal cells; β_1 death or differentiation rate (per cell per year) of normal cells; μ_1, rate (per cell per year) at which the first event occurs. α_2, β_2, and μ_2 are defined similarly. This figure was adapted from (Moolgavkar and Knudson, Jr., 1981).

distribution with expectation $\int_0^t \mu_1 X(s)ds$, where X(s) is the number of

normal cells at time *s* (Moolgavkar and Knudson, Jr., 1981).

From the MVK model, the incidence function *I(t)*, which is the rate that tumors occur in previously tumor-free tissue, can be computed as

$$I(t) \approx \mu_1\mu_2 \int_0^t X(s)\exp[(\alpha_2 - \beta_2)(t-s)]ds \qquad (2.1)$$

The details of the mathematical derivation of the MVK model were discussed by Moolgavkar and colleagues (Moolgavkar, 1979; Moolgavkar and Knudson, Jr., 1981). The age-specific incidence rate at age *t* per 100,000 individuals in a population is then calculated by $I(t) \times 10^5$ (Moolgavkar and Knudson, Jr., 1981).

The MVK two-stage model was incorporated with the phenomena of "initiation" and "promotion" in carcinogenesis and resulted in successful predictions. In the framework of the MVK model, the initiator, which acts at the level of DNA as mutagens, affects the transition rate of the first event (μ_1), whereas the promoter, which acts at the cell surface to cause cell proliferation, increases the proliferation rate of intermediate cells, *i.e.* increases α_2, decreases β_2, or both (Moolgavkar, 1983). By incorporating hormones and cigarette smoke as promoters, the model made a good quantitative description of the epidemiology of breast and lung cancers,

respectively (Moolgavkar, 1983).

The analytical solutions of the MVK two-stage model have been limited by the number of piecewise-constant intervals, within which the birth and death rates are assumed to be constants. The computer simulation of the clonal growth cancer model proposed by Conolly and Kimbell (Conolly and Kimbell, 1994) eliminated this constraint. The computational efficiency could be highly increased if the growth of intermediate cells are treated as stochastically for clones with smaller population and assumed to be deterministic for clones with larger population. The improvement on the MVK model achieved by computer simulation made this model even more applicable to carcinogenesis studies.

2.3 SHE cell transformation assay

The Syrian hamster embryo (SHE) cell transformation system was first used to examine the carcinogenicity of chemicals by Berwald and Sachs (Berwald and Sachs, 1963; Berwald and Sachs, 1965). SHE cells have a stable and diploid karyotype. Syrian hamsters contain 44 chromosomes, which are similar in morphology and number to human chromosomes (Barrett, 1979). SHE cell cultures are prepared from whole embryos and contain a mixture of cell types. Some cell types in the mixture have the capacity to undergo neoplastic transformation, whereas others have the

ability to metabolize chemical carcinogens (Barrett, 1979). *In vivo*, the liver is able to metabolize relatively innocuous precursors to toxic metabolites, a process called metabolic activation (Ballantyne *et al.*, 1995). The ability of cells *in vitro* to metabolize chemical carcinogens is an important consideration when extrapolating carcinogenicity data from an *in vitro* system to humans.

With the feature of multistep neoplastic progression, the SHE cell transformation system has been widely used to study the carcinogenesis process, which was believed to include initiation, promotion, and progression stages *in vivo* (Boyd and Barrett, 1990). This system also provides the advantages of a low frequency of spontaneous transformation and readily demonstrable neoplastic transformation upon treatment with chemical carcinogens (Barrett, 1993).

The pathway of SHE cell neoplastic development following carcinogen treatment was best described by Barrett (Barrett, 1993) and shown in Figure 2.2. The earliest phenotypic alteration is morphological transformation, characterized by a disorganized and crisscrossed growth pattern in colonies. Morphological transformation was not included in the pathway because it is not essential for progression to later neoplastic phenotypes, although it is associated with an increased probability of the neoplastic progression (LeBoeuf, Kerckaert, Aardema, and Gibson, 1990).

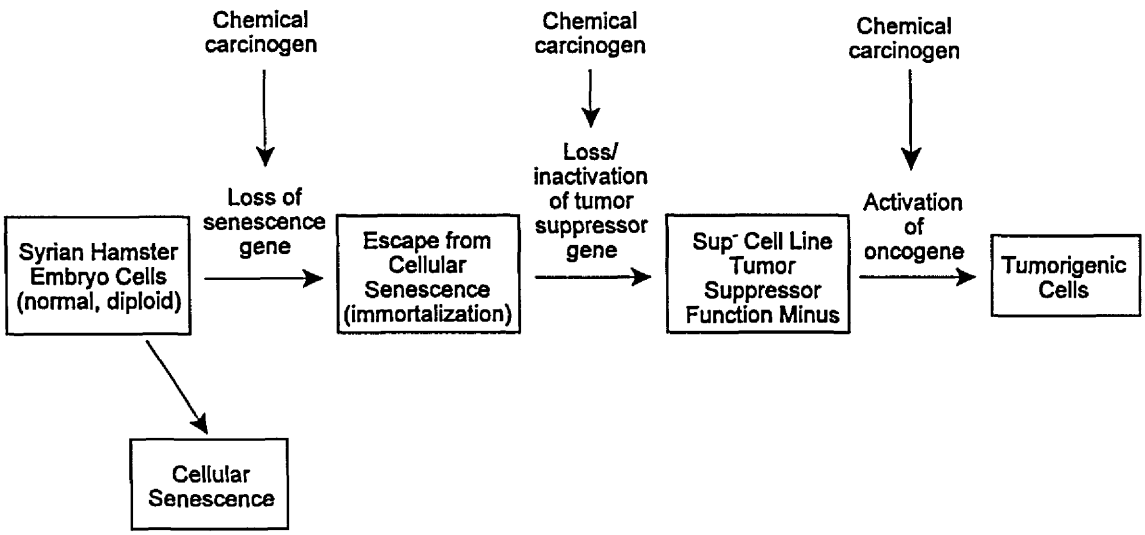

Figure 2.2. Pathway of Syrian hamster embryo cell neoplastic development

Normal cells in culture cease proliferation and become senescent after a limited number of cell divisions. At least three genetic changes must occur before the normal cells become tumorigenic. This figure was adapted from (Barrett, 1993; Preston *et al.*, 1994)).

Normal cells in culture cease proliferation after a limited number of cell divisions, a process called cellular senescence. Some cells lose senescence genes and become immortal, which is a necessary step for malignant progression. Cellular senescence is believed to be controlled by senescence genes which are activated at the end of the life span of normal cells and cause a block to DNA synthesis via down-regulation of cell cycle control (Barrett, 1993). Malfunction of these genes allow cells to escape cellular senescence. Senescence genes have been mapped in some chromosomal regions, but have not been identified yet (Barrett, 1993).

At least two additional genetic changes must occur before the immortal cell lines become tumorigenic. The changes include (1) loss or inactivation of a tumor suppressor gene followed by (2) activation of an oncogene (Barrett, 1993; Koi and Barrett, 1986). Cell hybrids between carcinogen-induced immortal and tumorigenic cells were formed to determine the inactivation of the tumor suppressor gene (Koi and Barrett, 1986). Cells retain the ability to suppress tumorigenicity in early passages of immortal cell lines (sup^+); this ability was reduced or lost in later passages (sup^-) (Koi and Barrett, 1986). The phenotype of the sup^- cell lines is the ability of cells to grow in soft agar in the presence of mitogenic stimuli (Koi *et al.*, 1989; Preston *et al.*, 1994). The tumor suppressor genes inactivated in SHE cell transformation system remain unidentified; candidates include the putative

tumor suppressor genes *H19* and *TM-1* (Preston, Lang, Maronpot, and Barrett, 1994; Hao *et al.*, 1993; Prasad *et al.*, 1993).

The oncogenes activated before cells become tumorigenic in this model (Figure 2.2) include the Ha-*ras* proto-oncogene and non-*ras* genes (Barrett, 1993; Gilmer *et al.*, 1988). The tumorigenicity of cells are determined by the ability to form progressively growing tumors in newborn hamster or immunocompromised mice.

Mechanistic studies of genetic and cellular basis of the SHE cell transformation system are still in progress. In this particular project, we approached this system from a quantitative perspective by incorporating cancer modeling with the MVK two-stage model.

2.4 Metals tested in this project

Arsenic, chromium, lead, and a mixture of these three metals were tested using SHE cell transformation assay. The background of these metals are discussed below.

2.4.a Arsenic

Arsenic is a ubiquitous constituent in the earth's crust and has been used by human since as early as 2000 B.C. It is also a common soil and water contaminant that has been found in at least 781 of 1,300 sites on

National Priorities List identified by EPA (ATSDR, 1993a). Arsenic can exist in three valence states: elemental (zero oxidation state), trivalent (arsenite), or pentavalent (arsenate) arsenic (Jolliffe, 1993). The toxicity of arsenic to mammals depends on the valence state, the physical state, and the rates of absorption and elimination. Trivalent arsenite is more toxic than pentavalent arsenate. The toxicity of inorganic arsenic is usually greater than organic arsenic. Arsine gas (AsH_3), which is used as a dopant in the production of arsenic semiconductors, is the most toxic of all the arsenical compounds (Jolliffe, 1993).

Arsenical compounds have been used in medicine, electronics, agriculture, and wood preservation. For medicinal applications, Fowler's solution (1% potassium arsenite), were used to treat a variety of diseases, *e.g.* psoriasis and syphilis, before 1940. Arsenicals are still used in the medicine of sleeping sickness today (Jolliffe, 1993). Because the use of III-V semiconductors are increasing, gallium arsenide (GaAs) and indium arsenide (InAs) use in the electronics industry are expected to increase (Yamauchi and Fowler, 1994). Therefore, environmental pollution of arsenic by these industries is inevitable. Ingesting arsenic-containing water and food is the main route of arsenic exposure for general population. Arsenic toxicity caused by drinking the well water contaminated by natural sources was reported in the United States, Taiwan, Germany, the United Kingdom, Chile,

and Argentina (ATSDR, 1990a).

Arsenite inhibits critical sulfhydryl-containing enzymes and can cause overt toxicity results (ATSDR, 1990a). Nevertheless, arsenate can competitively substitute for phosphate and causes hydrolysis of high energy bonds, as a results, energy needed for cellular metabolism can lose (ATSDR, 1990a). Interconversion of trivalent and pentavalent arsenic can be caused by oxidation-reduction reactions *in vivo*. Arsenite can be biomethylated to methylarsonic acid and dimethylarsinic acid for renal excretion (Morton and Dunnette, 1994).

Chronic arsenic inhalation is strongly related to lung cancer in human. Chronic ingestion of arsenicals is also closely associated with human skin cancer and possibly cancers of the liver, kidney, lung, bladder, and colon. However, the linkage of cancers to arsenic exposure could not be substantiated in experimental animals (ATSDR, 1990a).

Among other health effects, Blackfoot disease, a peripheral vascular disease, was caused by drinking arsenic contaminated well water in Taiwan. Raynaud's phenomenon and acrocyanosis were reported in Chile as a result of the contamination of the city's drinking water supply (ATSDR, 1990a). Hyperpigmentaion, hyperkeratosis, anemia, and leukopenia were also reported to be associated with chronic arsenic exposure (ATSDR, 1990a).

2.4.b Chromium

Chromium is commonly used in several industrial processes and has been found in at least 115 of 1300 National Priorities List sites that were identified by the EPA (ATSDR, 1993b). Chromium has two main forms, trivalent (Cr[III]) and hexavalent (Cr[VI]), that are encountered in biological systems (Cohen *et al.*, 1993). Cr(III) compounds exist naturally in chromite ore, whereas Cr(VI) compounds rarely occur naturally and are produced from industrial processes, such as chrome plating, leather tanning, pigments, as an antirust agent for water-cooled machinery (Costa, 1997).

Cr(III) is an important dietary element at very low concentration (ATSDR, 1990b). The trivalent chromium is believed to play an essential role in the metabolism of insulin, in the form of "glucose tolerance factor" (GTF) which is a complex of Cr(III), nicotinic acid, and possibly amino acids (ATSDR, 1993c). Cr(III) also plays an important role in the metabolism of fat and cholesterol (ATSDR, 1990b).

Cr(VI) is not needed by human bodies and is extremely toxic. Under physiological conditions, Cr(VI) exists as chromate anion (CrO_4^{-2}), which structurally resembles several tetrahedral physiological anions, such as PO_4^{-3} and SO_4^{-2}. As a result, Cr(VI) is readily transported into all cells of the body using the general anion transport system (Cohen, Kargacin, Klein, and Costa, 1993; Costa, 1997).

Inhalation, ingestion, and dermal absorption are the routes by which chromium enters human body. Cr(VI) is more readily absorbed by body than Cr(III) in all of these three routes because Cr(VI) can penetrates cell membranes easily. After entering the body, Cr(III) tends to bind to plasma proteins such as transferrin, an iron-transporting protein (Cohen, Kargacin, Klein, and Costa, 1993). In contrast, by using preexisting anion transport mechanisms, Cr(VI) crosses cell membranes and is reduced to Cr(III) inside the cell (ATSDR, 1990b; Cohen, Kargacin, Klein, and Costa, 1993). As a result, Cr(III) accounts for most of the chromium in the body. Bone marrow, lungs, lymph nodes, liver, kidney, and spleen have the greatest uptake of Cr(III) (ATSDR, 1990b).

A variety of health effects have been reported for environmental exposure to chromium. In Woburn, MA, a fourfold increase in leukemia was caused by a high level of Cr(VI) in drinking water consumed by children (Costa, 1997). The level of DNA-protein crosslinks was found to be increased in people living in Jersey City, NJ, where chromium-containing slag was used as landfill in residential areas (Costa, 1997). Other effects caused by exposing to chromium includes respiratory distress, asthma, skin rashes (Costa, 1997), dermatitis with eczema, liver abnormalities, renal tubular necrosis, and, last but not least, lung cancer (ATSDR, 1990b).

It has been firmly established in epidemiological studies that an increased incidence in respiratory cancers develops following exposure to Cr(VI) particles and dusts in industrial processes (Cohen, Kargacin, Klein, and Costa, 1993). Inhaled Cr(VI) has been classified as a human carcinogen by EPA and the International Agency for Research on Cancer (ATSDR, 1990b). There is not sufficient evidence indicating that Cr(III) is a human carcinogen.

In more recently published epidemiological studies, evidence shows that soluble Cr(VI) also induces other types of cancers besides respiratory cancers, including cancers in kidney, urinary tract, bladder, testes, stomach, prostate, and brain (Costa, 1997). Due to the fact that Cr(VI) can be absorbed readily by inhalation, ingestion, and skin, these results are expected (Costa, 1997).

Depite the epidemiological evidence indicating that Cr(VI) causes human cancers, there is no animal model with natural exposure routes (inhalation, ingestion, or dermal absorption) that has shown unequivocally positive results for carcinogenicity of Cr(VI) (ATSDR, 1990b). However, intratracheal or intrabronchial implantations, intratracheal instillation, and subcutaneous implantation of Cr(VI) compounds did induce the formation of tumors at the site of application in some studies (Cohen, Kargacin, Klein, and Costa, 1993; ATSDR, 1990b).

2.4.c Lead

Since lead has been used from the beginning of civilization, it can be found in every part of our environment, including in at least 922 of 1300 National Priorities List sites identified by the EPA (ATSDR, 1993d). Most of the lead in our environment was from man-made sources such as batteries, metal solder and pipes, ammunition, roofing, and x-ray shielding devices. Earlier, lead also existed in gasoline, paints, ceramic products, and caulking, but the usage was reduced recently due to the health concerns (ATSDR, 1993d). Humans could be exposed to lead from drinking water transported by lead-soldered plumbing, eating food grown on soil contaminated by lead (unleaded gasoline is not required for agricultural vehicles), eating lead-containing paint chips, and ingesting or breathing contaminated soil, air, or water near waste sites (ATSDR, 1993d; ATSDR, 1992).

Organic lead that is absorbed by the body through inhalation and skin contact is metabolized by the liver. Inorganic lead enters the body through inhalation and ingestion without undergoing biologic transformation (ATSDR, 1992). Smaller particles of the inhaled lead deposited in lower respiratory tract are completely absorbed. Ten to 15% of ingested lead, as well as larger particles of the inhaled lead which are deposited in upper respiratory and moved to gastrointestinal tract by ciliary action and swallowing, are absorbed (Putnam, 1986). After being absorbed, lead is distributed to three

compartments, blood, soft tissues (kidney, brain, liver, and bone marrow), and bones (ATSDR, 1992). Bone contains approximately 95% of the total body burden of lead and serves as an inert pool. Bone lead, which has a half-life more than 25 years, can cause elevated blood levels over time, especially when the body is under physiologic stress.

Lead can cause a variety of health effects ranged from relatively mild effects to chronic disease and even death. Based on animal studies, the Department of Health and Human Services determined lead acetate and lead phosphate may reasonably be anticipated as carcinogens (ATSDR, 1993d), whereas carcinogenicity of lead in humans is still undetermined due to inadequate evidence. Lead also causes central nervous system effects in adults, expressed by behavioral changes, impaired concentration, and fatigue (ATSDR, 1992). Studies showed that children with high tooth lead levels had larger deficits in speech and language processing, psychometric intelligence scores, and attention than children with lower tooth lead levels (ATSDR, 1992). For hematological effects, lead inhibits the production of hemoglobin by interfering several enzymatic steps in the heme pathway, which results in anemia due to the decreased number of red blood cells. For reproductive effects, lead causes sterility, increased rate of stillbirths, and increased rate of miscarriages (Putnam, 1986).

CHAPTER 3

Materials and Methods

3.1 Cell culture techniques

All cell culture techniques and protocols were modified from previous studies in our laboratory (Smith, 1997) and those from Dr. LeBoeuf's laboratories at The Proctor & Gamble Company (LeBoeuf, Kerckaert, Aardema, and Gibson, 1990) for modeling purposes.

3.1.a Culture medium

Dulbecco's Modified Eagle's Medium-LeBoeuf's modification (DMEM-L; Quality Biological Inc., Gaithersburg, MD) was used throughout the study. DMEM-L is a modification of low glucose (1000 mg/L) while DMEM is with an equimolar concentration of $MgCl_2$ replacing $MgSO_4$, 0.75 g/L $NaHCO_3$, and a reduced concentration of phenol red (5 vs. 15 mg/L) (LeBoeuf, Kerckaert, Aardema, and Gibson, 1990). Twenty percent of fetal bovine serum (FBS; Summit Biotechnology, Ft. Collins, CO) was used in the medium for clonal growth and 10% of FBS was used in the medium for serial passage of cell lines. L-Glutamine (Life Technologies, Grand Island, NY) was

added to achieve 4 mM final concentration. Penicillin-Streptomycin (5000 units/mL penicillin/5000 μg/mL streptomycin; Life Technologies) was used as antibiotics and diluted at 1:100 into the solution. The complete medium yields a pH of 6.7 while incubated at 37 °C with 10% CO_2.

3.1.b Isolation of primary embryo cells

Golden Syrian hamsters (Charles Rivers Laboratories, Kingston, NY) at gestation day 13 were the sources of the primary embryo cells. The methods were previously described by Smith (Smith, 1997) and LeBoeuf et al. (LeBoeuf *et al.*, 1989; LeBoeuf and Kerckaert, 1986). Twenty-five to 30 embryos were obtained from three pregnant animals which were sacrificed by CO_2 asphyxiation. Embryos were then decapitated, eviscerated, and washed in calcium-magnesium-free Hank's Balanced Salt Solution (CMF-HBSS; Life Technologies) containing Penicillin-Streptomycin (200 units/mL penicillin/200 μg/mL Streptomycin; Life Technologies). To collect cells, the embryo tissue pieces were dissociated with CMF-HBSS containing 1.25% (v/v) trypsin (40X Enzar-T, Intergen Company, Purchase, NY) and 2.5% (v/v) pancreatin (4X NFU, Life Technologies).

Cell viability and density were counted by exclusion of Trypan blue stain (0.4%, Life Technologies) on a Hemacytometer. Twenty million viable cells were seeded in each T-150 culture flask (150 cm^2 tissue culture flask;

Corning). After 24 hours, cells were detached from the flasks using 5 mL of Trypsin-EDTA (0.05% Trypsin, 0.53 mM EDTA.4Na; Life Technologies) at 37 °C for five minutes. The cells pooled from flasks were counted and diluted to 2×10^6 cells per mL in culture medium with 7.5% (v/v) dimethyl sulfoxide (DMSO; Hybri-Max, Sigma Chemical). One-mL aliquots of this cell suspension were frozen in 2-mL cryogenic tubes (Wheaton) at -80 °C for 24 hours and then transferred to liquid nitrogen storage for up to six months.

3.1.c Cell preparation for clonal growth

Syrian hamster embryo (SHE) cells were exposed to chemicals for 48 hours during the clonal growth period. Two sets of cells were required for clonal growth. First, a feeder layer, which was irradiated to cease proliferation, was seeded, and then a target layer was plated out above the feeder layer and exposed to chemicals. For feeder layer preparation, a vial of cryopreserved SHE cell isolate was thawed and seeded in a T-150 culture flask with 30 mL of culture medium, then incubated at 10% CO_2, 37 °C, and saturated humidity. The cells were re-fed with fresh medium after four hours to eliminate the DMSO used in cryopreserving. Three days later, cells were trypsinized and gamma irradiated at 5000 rads with a Sherpard & Son Mark 1, 6000 Curie ^{137}cesium source. After irradiation, cells were spun down at $900 \times g$ for 10 minutes, resuspended in 10 mL medium, counted, and diluted

to 10000 cells per mL. This dilution was plated out in 100-mm petri dishes (Falcon) at 10 mL per dish as the feeder layer.

To prepare the target cells, another vial of SHE cell isolate was thawed and seeded in T-25 culture flask with 5 mL of culture medium on the same day with feeder layer being plated out. These cells were re-fed with fresh culture medium after four hours and grown overnight. The target cells were then trypsinized, counted, and diluted to 2000 cells per mL. One hundred and two hundred micro liters of this solution, for control and chemical-treated groups, respectively, were added to each 100-mm petri dish containing feeder layer and 10 mL culture medium. These amounts achieved 200 and 400 target cells per dish for control and chemical-treated groups, respectively. After 24 hours, the cells were dosed with the individual test metals and the metal mixture in 5 mL of medium and incubated for 48 hours. The culture medium containing chemicals was then replaced and the cells were allowed to grow for seven days.

3.1.d Colony isolation and passage

After seven days of clonal growth, approximately 30 colonies were selected randomly and isolated from control and metals-treated groups, and 18 colonies from BaP-treated group. To isolate colonies, plastic cloning cylinders (Sigma Chemical) were placed on selected colonies and the cells in

the cylinders were washed with CMF-HBSS. The cells were then trypsinized with drops of Trypsin-EDTA and transferred to separate 60-mm petri dishes with 4 mL of culture medium, one colony per dish. It was important at this stage to be able to analyze independent colonies, based on the assumption that a colony is the expansion of a single parental cell.

Following the colony isolation, cells needed to be passaged once a week. For the control group, each isolate was re-plated at 4×10^4 cells in 4 mL of culture medium per 60-mm petri dish. For other groups, 1/20 of cells were re-plated in each 60-mm petri dish containing 4 mL of culture medium. Each isolate was re-plated in parallel in two dishes to prevent the loss of isolates due to contamination. Cell lines were determined to be senescent when they did not need to be passaged for more than three weeks and expressed cytoplasmic spreading.

3.1.e Growth inhibition study

During the experiments to induce immortal SHE cell lines in our laboratory, arsenic was found to inhibit the growth of SHE cells rather than extend the life span. As a result, an experiment was designed to study the dose-response growth inhibition caused by arsenic. A vial of cryopreserved SHE cells was seeded in T-150 flask and re-fed after 4 hours. Following three days of incubation, cells were re-plated in 60-mm petri dishes at

4×10^4 cells per dish and incubated for 24 hours. Cells were then exposed to arsenic for two days at four concentrations, *i.e.* LC_{50} of arsenic to SHE cells obtained from cytotoxicity studies (Section 3.2) and three concentrations below it. The cells were washed and passaged after the exposure. The procedures of passaging cells were identical to those described in the previous sections.

3.2 Cytotoxicity study

To obtain the chemical treatment concentrations for our studies and model development, the toxicities of the selected metals (lead, arsenic, chromium) and the mixture of these three metals were assessed in SHE cells using the MTT (3-[4,5-Dimethylthiazol-2-yl]-2,5-diphenyltetrazolium bromide; thiazolyl blue) assay. The chemicals used in this study were lead acetate trihydrate, sodium m-arsenite, and the mixture of chromium chloride hexahydrate [chromium(III)] and chromium oxide [chromium(VI)] in a 1:1 ratio; all chemicals listed above were purchased from Sigma Chemical Company. SHE cells were plated at 96 well tissue culture plates at 6000 cells per well and incubated for 24 hours. Single metals at graded concentrations were added to the medium and cells were treated for 48 hours. Equi-toxic concentrations were used in the mixture studies followed by the single metal studies.

After treatment, the cells in each well were incubated with 50 μg of MTT (Sigma Chemical) for four hours. MTT yields a yellowish solution when dissolved in culture medium. Dehydrogenase enzymes in live cells could cleave the tetrazolium ring of MTT and convert it to insoluble purple MTT formazan (1-[4,5-Dimethylthiazol-2-yl]-3,5-diphenylformazan). Absorbance was read on a microplate reader at 550 nm after the MTT formazan crystals were dissolved by 100 μL of DMSO. LC_{50} is defined by the concentration at which the chemical results in 50% inhibition of absorbance at 550 nm and was determined by log plots of percentage of control absorbance versus metal concentration.

3.3 Cell division rate measurement

Cell division rates were measured using bromodeoxyuridine (BrdU) incorporation with propidium iodide staining, which allows for the calculation of potential doubling time (T_{pot}). T_{pot} is a measure of cell cycle time that takes cell growth fraction, but not cell loss, into account (Steel, 1977; Wilson, 1994). After obtaining T_{pot}, the cell division rate, α, was calculated from the equation

$$\alpha = \frac{\ln 2}{T_{pot}} \qquad (3.1)$$

3.3.a Potential doubling time method

The division rate was estimated from the potential doubling time that could be calculated by Equation 3.2,

$$T_{pot} = \lambda \cdot \frac{T_s}{LI} \qquad (3.2)$$

where T_S is the period of DNA synthesis, LI (labeling index) is the fraction of cells synthesizing DNA, and λ is a correction factor for the nonlinear distribution of cells through the cell cycle (Steel, 1977; Wilson, 1994).

Potential doubling times were measured in flow cytometry by pulse-labeling cells with bromodeoxyuridine (BrdU) and detected its incorporation into DNA by the use of fluorescent antibodies. The cells were then counterstained by propidium iodide to measure the DNA content. Estimation of T_{pot} values relied upon distinction of cells in different stages of the cell cycle. The cell cycle contains four stages (Figure 3.1). The cell increases in size and prepares for DNA replication in the G_1 (gap one) phase. In the S (synthesis) phase, the cell replicates its nuclear DNA. In the next gap period (G_2 phase), the cell confirms that DNA replication is complete before it proceeds through mitosis (M), in which the cell finally divides into two daughter cells.

The results from a representative flow-cytometry study are shown in Figure 3.2 and discussed here to illustrate the method. Each window in

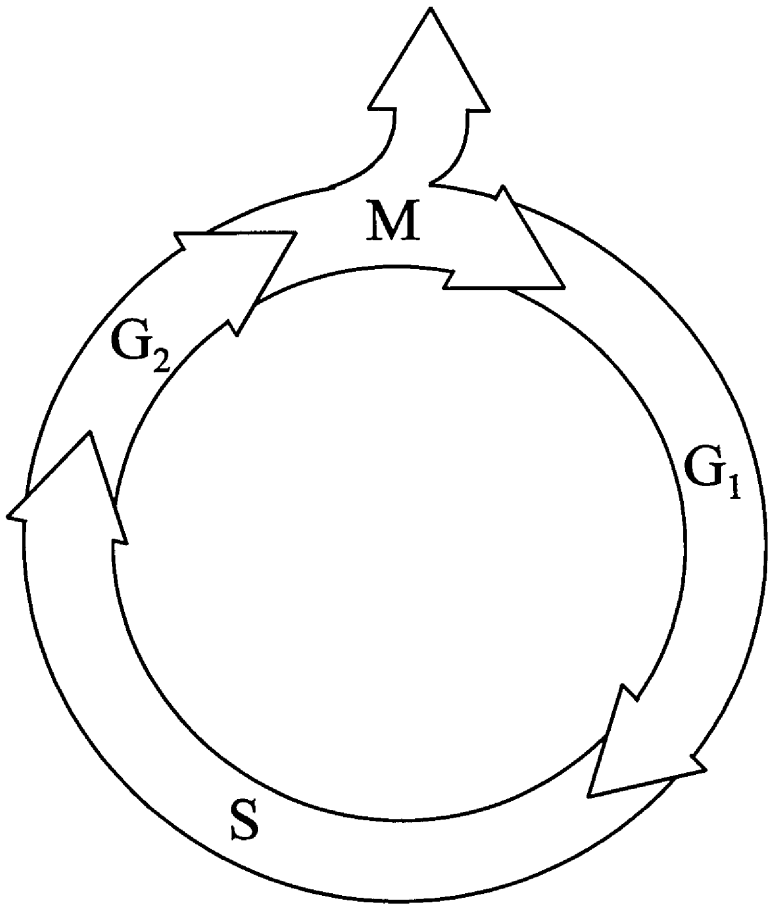

Figure 3.1. The four stages of a cell cycle

The cell cycle proceeds clockwise through four successive stages (G_1: gap 1 ; S: synthesis; G_2: gap 2; M: mitosis)

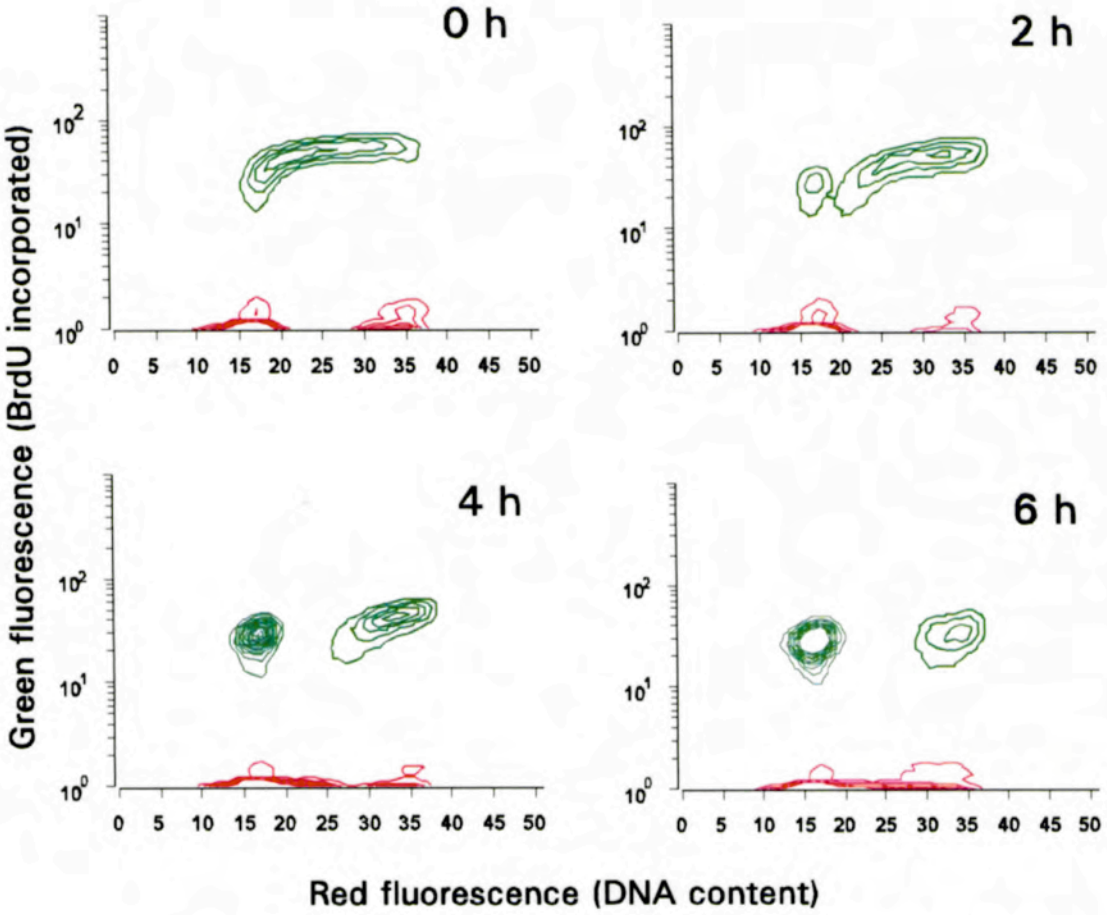

Figure 3.2. Bivariate histograms of BrdU incorporation versus DNA content

Panels present bivariate histograms obtained from cells stained at 0, 2, 4, and 6 hours after BrdU pulse-labeling. X-axis is intensity of red fluorescence (DNA content), y-axis is intensity of green fluorescence (BrdU incorporated). All cells were stained by propidium iodide with intensities proportional to DNA content, while cells in S phase during BrdU pulse-labeling were labeled by BrdU (green contours).

Figure 3.2 is a bivariate histogram containing the green fluorescence (BrdU incorporated) on y-axis and red fluorescence (DNA content) on x-axis. The left-top window presents the histogram immediately after BrdU pulse-labeling (0 hour). The cells labeled with BrdU (S phase) lay between two groups without green fluorescence, G_1 on the left and G_2/M on the right.

After two hours, the green population (S phase cells) moved to the right while a small population appeared as G_1 phase cells. That is because most of the BrdU-labeled cells moved through S phase to G_2/M and a small population were in or had completed mitosis and divided into daughter cells (*i.e.* G_1 cells). At later time points (*i.e.* four and six hours), there was an increasing number of cells that had divided and now appeared on the left side as G_1 phase cells.

T_S can be measured by the relative movement of the BrdU labeled cells through a certain region (Begg *et al.*, 1985). The relative movement (RM) is calculated as

$$RM = \frac{F_L - F_{G_1}}{F_{G_2/M} - F_{G_1}} \qquad (3.3)$$

where F_L represents the mean red fluorescence intensity of the BrdU labeled cells (Figure 3.3). F_{G1} and $F_{G2/M}$ are the mean red fluorescence intensity of G_1 and G_2/M cells, respectively. F_L is approximately in the middle of F_{G1} and

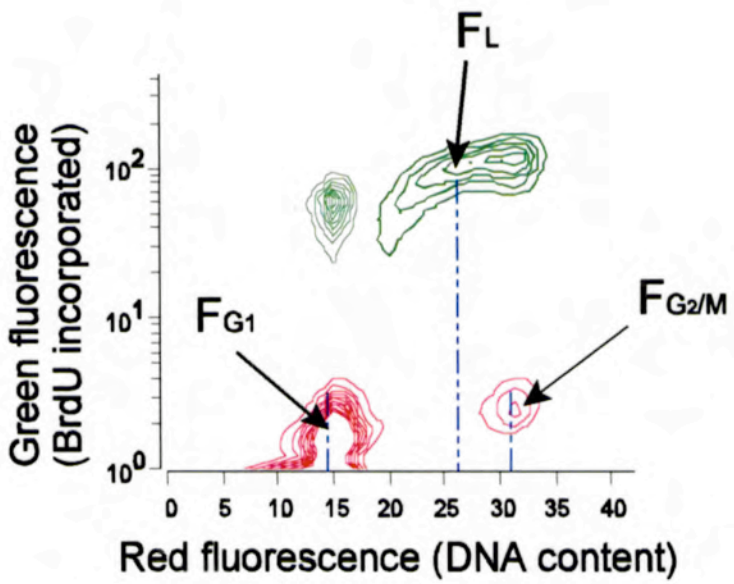

Figure 3.3. The schematic plot for the calculation of relative movement

Elements contained in Equation 3.3, used to calculated the relative movement, are indicated schematically. F_L represents the mean red fluorescence of the BrdU labeled cells. F_{G1} and $F_{G2/M}$ are mean red fluorescence of G_1 and G_2/M cells, respectively.

$F_{G2/M}$ at time zero, *i.e.* RM is approximately equal to 0.5. F_L will approach $F_{G2/M}$ as time passes and RM will be equal to one at T_S.

By setting RM equal to 0.5 at time zero (Begg, McNally, Shrieve, and Karcher, 1985), the DNA synthesis time can be calculated as

$$T_s = \frac{0.5}{RM - 0.5} \times t \qquad (3.4)$$

where t is the sampling time. Labeling index is calculated as the proportion of cells labeled by BrdU. By assuming λ equal to one, T_{pot} can be obtained from Equation 3.2.

3.3.b Bromodeoxyuridine/propidium iodide staining protocol

SHE cells were plated in parallel on 60-mm petri dishes at 4×10^4 cells per dish. After 72 and 120 hours, 10 μM of BrdU (Sigma Chemicals Co.) was used to pulse-label the cells for 20 minutes. Fresh medium was added to the cells after BrdU was removed, and the cells were grown for another 3 hours. BrdU-labeled cells were then trypsinized and fixed in 70% ethanol, which helped propidium iodide to penetrate the plasma membrane. Fixed cells could be stored in 70% ethanol at 4°C for months before staining.

The staining protocol was modified from Larsen (Larsen, 1994). The first step of staining was to partially denature DNA to allow access of the monoclonal antibody to its epitope on the incorporated BrdU. To achieve the

denaturation, 0.2 mg pepsin (Sigma Chemical Co.) was dissolved in each mL of 2N HCl and incubated with cells at 37 °C for 15 minutes. To terminate the denaturation, 1 M Tris (Trizma base, Sigma Chemical Co.) was added to the cells which were then washed with PBS. Monoclonal mouse anti-BrdU antibody (Dako) was added and incubated with cells for 30 minutes at room temperature. After the anti-BrdU antibody was washed out, fluorescein isothiocyanate (FITC)-conjugated rabbit anti-mouse antibody (Dako) was used to bind to anti-BrdU for 15 minutes at room temperature. For the last step of staining, 10 μg/mL of propidium iodide combined with 1 mg/mL of RNase were added to create specific DNA binding. Cells were filtered through 53-μm nylon mesh (Small Parts Inc., Miami Lakes, FL) before flow cytometric analysis.

3.4 Cell death rate measurement

The cell death rates were measured by staining cells with propidium iodide. This dye is only taken up by dead cells through the damaged membrane and is excluded by live cells (Ormerod, 1994). Propidium iodide binds to nucleic acids and fluoresces red after entering dead cells. By setting a gate in the forward angle light scatter (FALS), which is an indicator of cell size, debris and clumps could be excluded from flow cytometric measurement (Figure 3.4A). Cells screened by FALS were examined on the

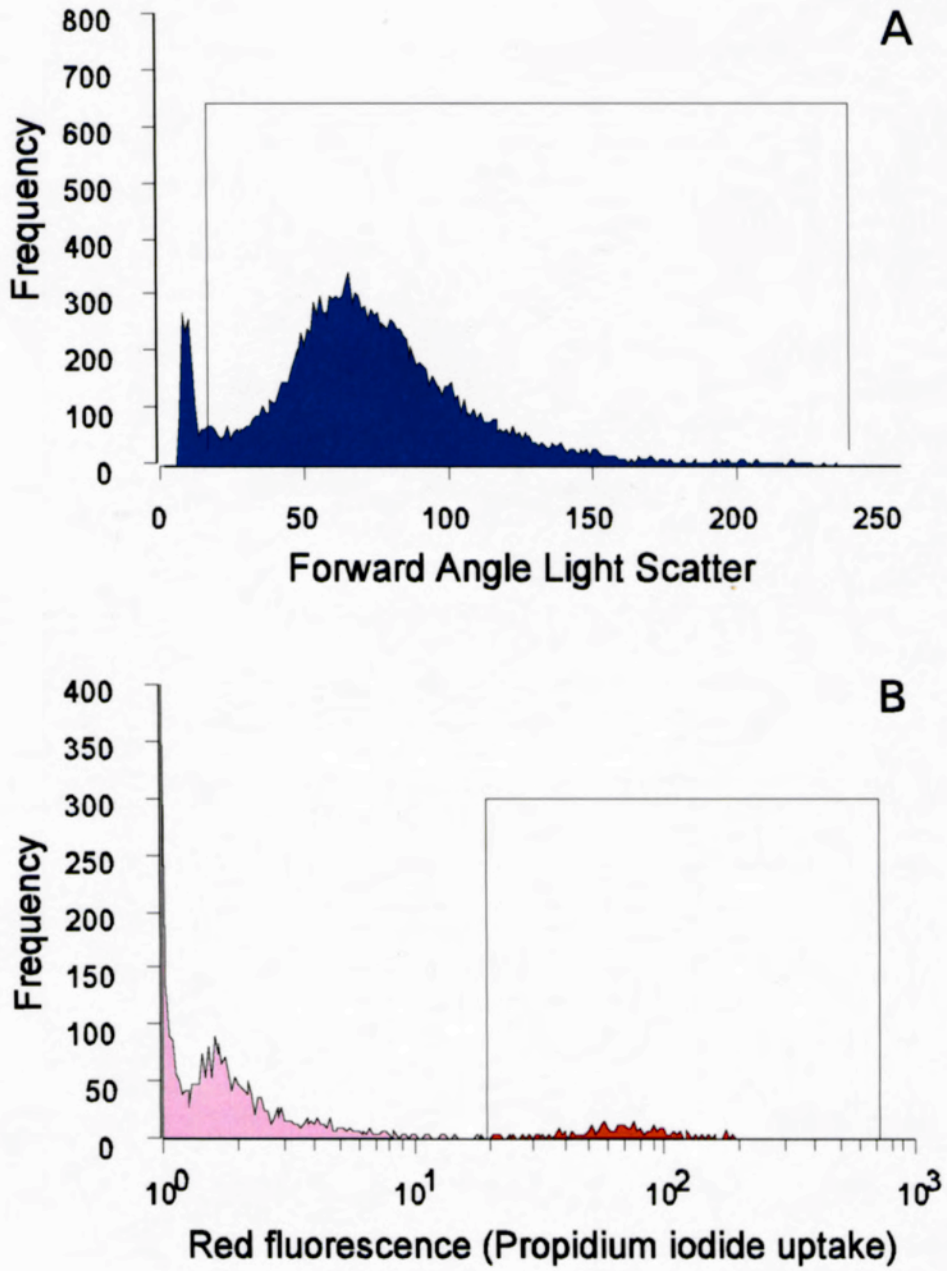

Figure 3.4. Histograms for death rate measurement

A: Cells screened by forward angle light scatter: cells in delineated area were analyzed for propidium iodide uptake (B). B: Dead cells, which take up propidium iodide, show bright red fluorescence (delineated area).

basis of their uptake of propidium iodide (Figure 3.4B), and the fraction of death cells in sample was obtained from these measurements.

SHE cells were plated in parallel at 40000 cells per dish. Samples were harvested at 72, 96, and 120 hours after plating. Two mL of Trypsin-EDTA was used to detach the cells at 37 °C for five minutes. In addition, medium from the culture and 3 mL of CMF-HBSS used to wash cells were collected since dead cells did not attach. After all cells were collected, they were shipped to the flow cytometry lab and centrifuged. The pellets were resuspended in 1 mL of 50 μg/mL propidium iodide and incubated at room temperature for five minutes. The stained cells were filtered through a 53-μm nylon mesh before flow cytometric analysis.

Since the flow cytometric measurement only provides the percentage of dead cells, the total number of cells were counted to allow calculation of the number of dead cells. A dish of cells was harvested at the same time and by same procedure as were the cells measured in flow cytometry. These cells were centrifuged, resuspended in 1 mL of culture medium, and counted in hemocytometer under the microscope.

3.5 Flow cytometric analysis

Samples were analyzed with an EPICS V cell sorter (Coulter, Miami, FL) interfaced to a Cicero data acquisition and display system (Cytomation,

Inc., Ft. Collins, CO). Cells were illuminated by an argon ion laser at 488 nm (500 mW). FITC fluoresces at wavelengths between 515 to 530 nm and propidium iodide fluoresces at wavelengths longer than 610 nm.

For division rate measurement, a gating on peak vs. integral fluorescence of the propidium iodide signal was set to eliminate clumped cells. Thirty thousand counts of nuclei were triggered by the signal of propidium iodide fluorescence.

For death rate measurement, the gating was set on forward-angle light scatter to eliminate debris and clumped cells. Twenty thousand cells were counted for each sample.

3.6 Computer and software packages

The simulation programs were written in MATLAB® (The MathWorks Inc., Natick, MA) and ACSL Tox (ACSL = Advanced Continuous Simulation Language; Pharsight Co., Mountain View, CA) software packages. The programs were executed using a Gateway P5-200 personal computer (Gateway, Inc., San Diego, CA).

CHAPTER 4

Results and Discussion

4.1 Toxicities of metals to SHE cells

The results of cytotoxicity studies of chromium, arsenic, and lead to Syrian hamster embryo (SHE) cells are shown in Figure 4.1 and 4.2. The calculated LC_{50} of chromium was 3.6 μM (Figure 4.1A) and that of arsenic was 5.4 μM (Figure 4.1B). Lead was not very toxic to SHE cells and killed fewer than 50% of the cells, even at the relatively high concentration of 1 mM (Figure 4.2A). As a result, 100 μM of lead was assumed to have equi-toxicity to the LC_{50}s of the other two chemicals, and this level was used in the metal mixture toxicity study. *I.e.*, multiple dilutions were made from the mixture of the LC_{50}s of chromium and arsenic, as well as 100 μM of lead (Figure 4.2B). The LC_{50} estimated for the mixture was at the individual concentrations of 2.2 μM of chromium, 3.2 μM of arsenic, and 60 μM of lead. These results show that a mixture of the three metals exhibited less-than-additive toxicity, suggesting antagonistic interaction at the level of cell killing.

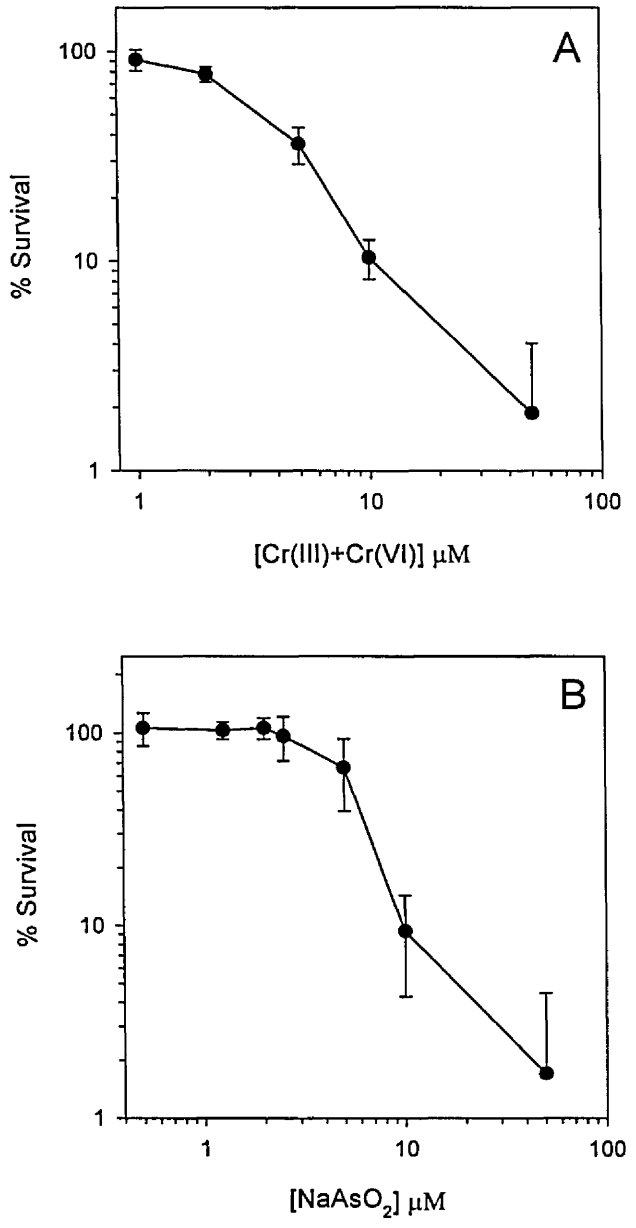

Figure 4.1. Cytotoxicity studies of chromium and arsenic to SHE cells

Cytotoxicity of chromium (A) and arsenic (B) to SHE cells were analyzed by MTT assay. The estimated LC_{50}s were 3.6 μM for chromium (A) and 5.4 μM for arsenic (B).

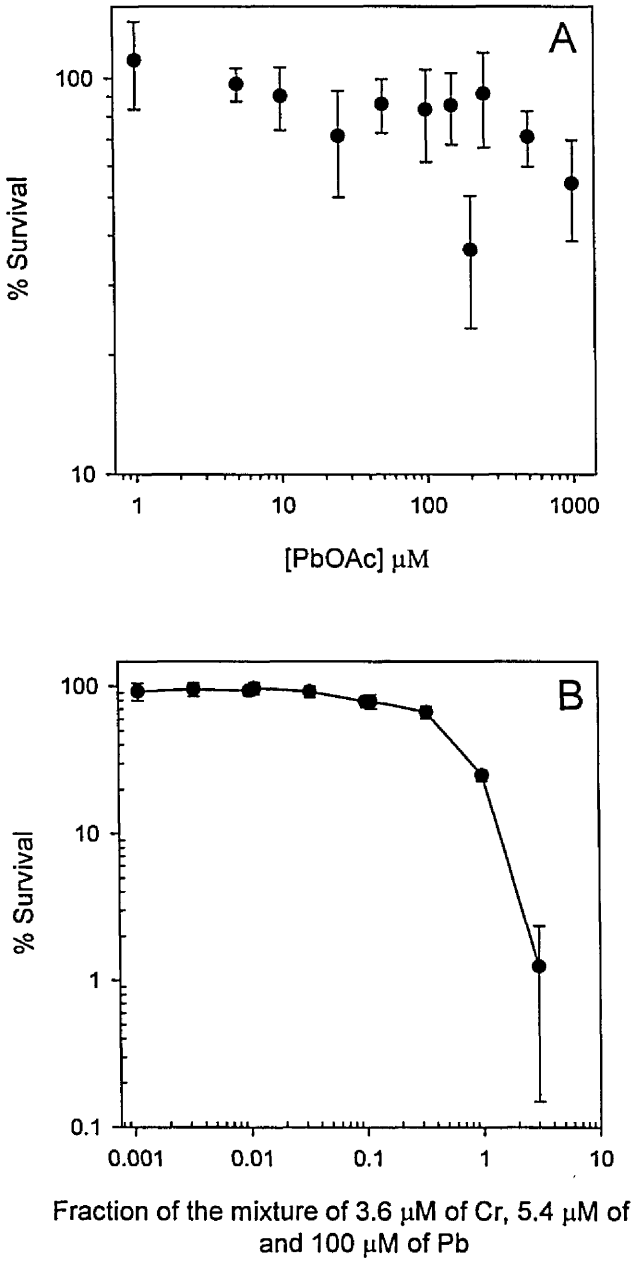

Figure 4.2. Cytotoxicity studies of lead and metal mixtures to SHE cells

Cytotoxicity of lead (A) and metal mixtures (B) to SHE cells were analyzed by MTT assay. For the metal mixture study, multiple dilutions were made from the mixture of the LC_{50}s of Cr and As, as well as 100 μM of Pb. The estimated LC_{50} for the mixture was at the individual concentrations of 3.2 μM of As, 2.2 μM of Cr, and 60 μM of Pb.

4.2 Attempted induction of immortal cell lines

Separate cultures of SHE cells were treated by the LC_{50}s of chromium, arsenic, and the metal mixture, and by 100 μM of lead for two days. Approximately 30 colonies from each chemical treatment were isolated and attempted for their ability to become immortal cells following serial passages. All cell isolates became senescent before the completion of 21 passages, which was calculated to be the equivalent of 112 population doublings. Senescent cells were observed to be morphologically distinguishable from normal cells (Figure 4.3). Senescent cells were much larger than normal cells and were characterized by cytoplasmic spreading, while normal cells grew in a flowing manner. The life spans of cell isolates, which were defined as the population doublings cells have grown until senescence, were shown in Table 4.1. All of the As-treated cell isolates became senescent at the second passage, and none of them proliferated for more than 22 population doublings, while at least one cell isolate from each of the other three treatment groups grew for more than 58 population doublings. These results showed that As at 5.4 μM inhibited the growth of SHE cells. The cell isolate with longest life span in this experiment lasted for 112 population doublings. It was treated with benzo[a]pyrene (BaP), our positive control agent for immortalizing SHE cells (LeBoeuf, Kerckaert, Aardema, and Gibson, 1990). The cell isolates that lasted longest for Cr and Pb grew for 69 and 101

Normal Cells

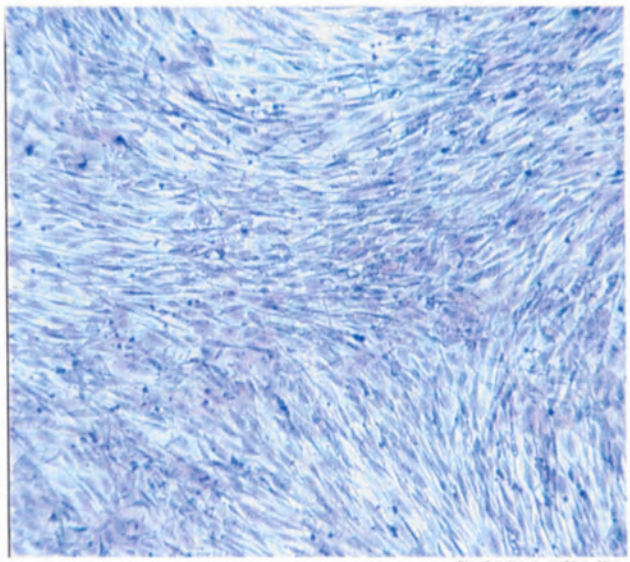

Ctrl15p3 1/21/99

Senescent Cells

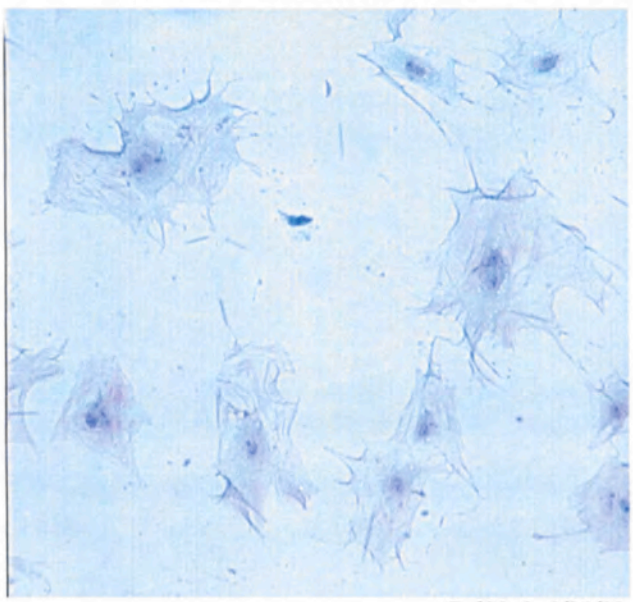

Ctrl29p3 1/21/99

Figure 4.3. Examples of normal and senescent SHE cells

Normal cells have fibroblast characteristics when confluency was reached. Senescent cells were much larger than normal cells and expressed cytoplasmic spreading.

population doublings, respectively. No additive effect was observed in the mixture-treated cells, which included one isolate with 58 population doublings.

Thus, none of the treatments induced immortal cells. The reason that immortal cell lines were not induced from the positive control group could be the exposure period. The experimental protocol was adapted from LeBoeuf et al. (LeBoeuf, Kerckaert, Aardema, and Gibson, 1990), in which BaP successfully induced immortal SHE cell lines, except that a 2-day exposure was used in our laboratory instead of the 7-day exposure used by LeBoeuf et al. Using the 2-day exposure was based on the consideration of applying the model to volatile organic chemicals later. Two volatile chemicals, trichloroethylene and 1,2-dichloroethane, dissolved the plastic dishes in previous 7-day exposure studies from our laboratory (Smith, 1997). The shorter exposure might not have been sufficient for BaP to induce mutation under the culture conditions we selected.

Arsenic was found to inhibit the growth of SHE cells. Cells exposed to chromium, the metals mixture, and BaP showed smaller degrees of growth inhibition compared to cells exposed to arsenic. Lead did not inhibit the growth of SHE cells. Since arsenic exhibited the greatest impact on the growth of SHE cells, the following model development focused on the effect on cell growth induced by arsenic. The cell division and death rates

Table 4.1: Life Spans of Cell Isolates

Population Doublings	Number of cell isolates from each chemical treatment					
	As	Cr	Pb	Mixture	Control	BaP
15-20	25	21	6	21	7	15
20-25	5	6	17	7	10	1
25-30		1	2		7	
30-40			2	1	1	
40-50			1		2	
50-60			1	1	2	
60-70		2			2	
80-90						1
>100			1		1	1
Total	30	30	30	30	32	18

measured from control cells, while obtained from the experiments described above, were also used in the model development.

4.3 Growth inhibition study by arsenic

Arsenic was observed to inhibit the growth of SHE cells from the results described in Section 4.2. A dose-response study was designed to further study the growth inhibition effect caused by arsenic. Four graded concentrations of arsenic, 0.5, 1.0, 2.0, 5.4 μM, were used in this study, where the highest concentration was the LC_{50} of arsenic to SHE cells. SHE

cells were exposed to arsenic for 2 days and their life spans were determined following serial passages. Since there was no significant difference observed between the growth of cell isolates in the previous experiment (Section 4.2), cells were exposed to arsenic at the density of 4×10^4 cells per dish instead of 400 cells per dish which was used in clonal growth. Arsenic at 5.4 μM shortened the life span of SHE cells, and the cells only grew for 16 population doublings before becoming senescent (Figure 4.4). SHE cells exposed to lower concentrations, 0.5, 1.0, 2.0 μM, grew for more than 30 population doublings and did not show significant difference in growth from control cells.

Cellular senescence induced by arsenic has not been previously reported. However, arsenic was found to induce mitotic inhibition in Chinese hamster ovary cells (Lee *et al.*, 1986). Furthermore, *in vivo*, arsenic was observed to cause inhibition of the promotion of preneoplastic lesions in rats (Pott *et al.*, 1998) and to decrease tumor incidence in mice (Kanisawa and Schroeder, 1967), although the processes underlying these effects remain unknown. Mechanisms involved in the induction of cellular senescence by arsenic *in vitro* may also be responsible for the effects observed *in vivo*. Induction of cellular senescence has also been reported with exposure to radiation (Peters, 1996).

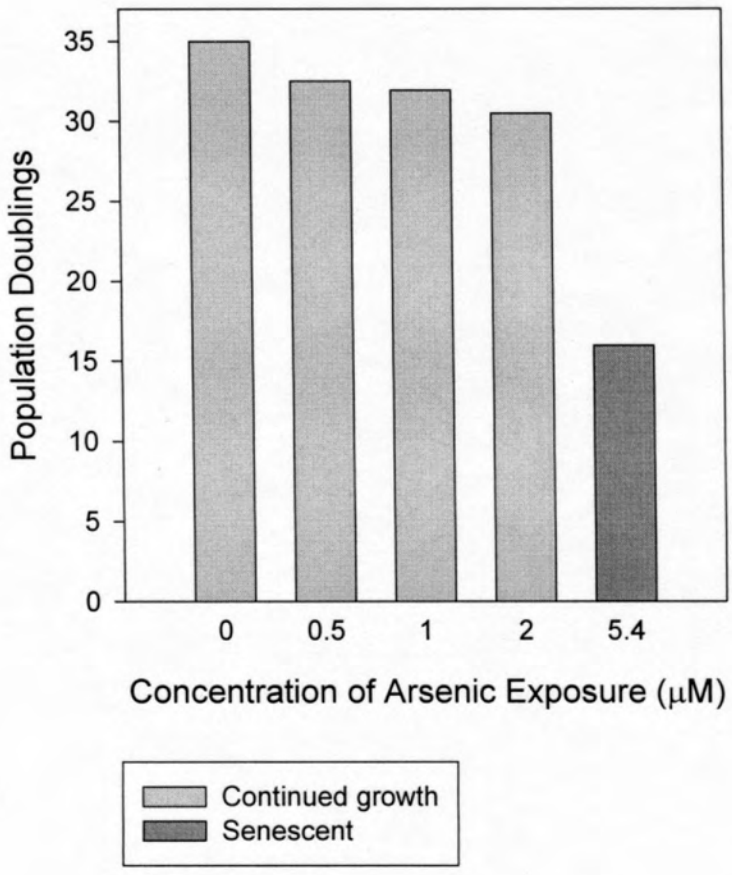

Figure 4.4. Effect of arsenic on the growth of SHE cells

Cells exposure to 5.4 μM of only grew for 16 population doublings before becoming senescent. All cells exposed to lower concentrations, 0.5, 1.0, 2.0 μM, grew for more than 30 population doublings and continued to grow beyond the numbers of population doublings shown above.

4.4 Cell division rates

The cell division rate (α) was calculated from the equation (Steel, 1977),

$$\alpha = \frac{\ln 2}{T_{pot}} \qquad (3.1)$$

where T_{pot} is the potential doubling time (Section 3.3). The calculations for T_{pot} values are shown in Appendix A. It was observed in normal cells that T_{pot} was a function of time after each passaging of the cells (Figure 4.5); this effect is presumed to be a result of "crowding". This result can be explained by the phenomenon of "density-dependent inhibition of cell division", which assumes that normal cells in culture stop dividing when a confluent monolayer is formed (Alberts *et al.*, 1994). Furthermore, a reduction of cell growth rates was detected when membrane contact occurred in a study conducted by video time-lapse microscopy in newborn rat dorsal root ganglion cells (Bandtlow *et al.*, 1990).

Short T_{pot} (high cell division rate) was observed while the cell density was low. As the cell numbers increased, longer T_{pot} (low cell division rate) was measured due to decreased space for cells to grow. Examples of the impact of cell density on T_{pot} are shown in Figure 4.6, where the measured T_{pot} was 13 hours on the third day after the cells were passaged (Figure

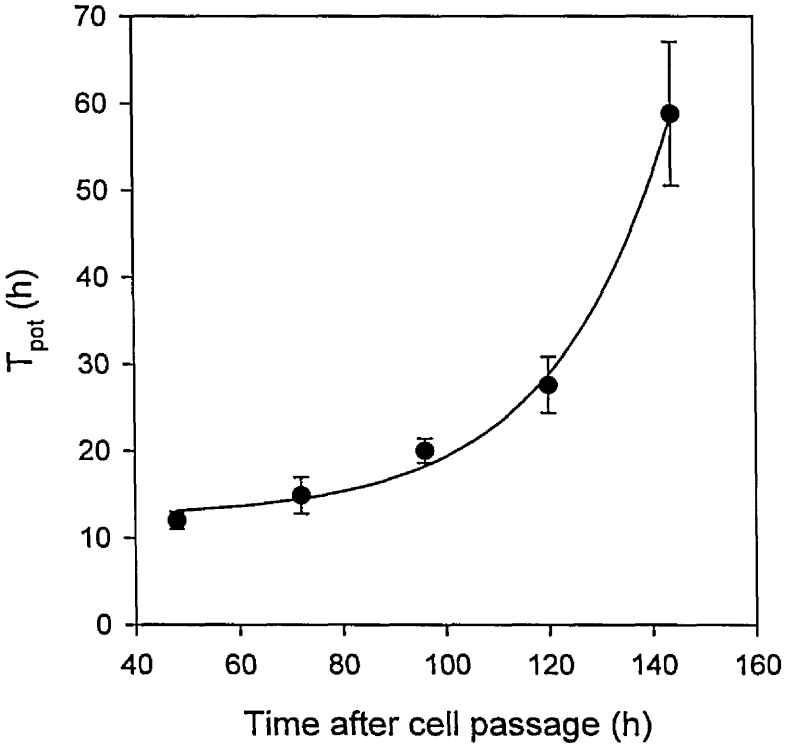

Figure 4.5. The change of potential doubling time (T_{pot}) as a function of time after cell passage in SHE cell culture system.

T_{pot} was observed to be a function of time after each passaging of the cells. The *dots* represent measured values with *error bars* representing ± one standard deviation. The *line* represents the result of nonlinear regression from the exponential equation $T_{pot} = 12.4 + 0.0913 * \exp(0.0432 * \text{time})$. This regression had a standard error of the estimate equal to 1.75 h.

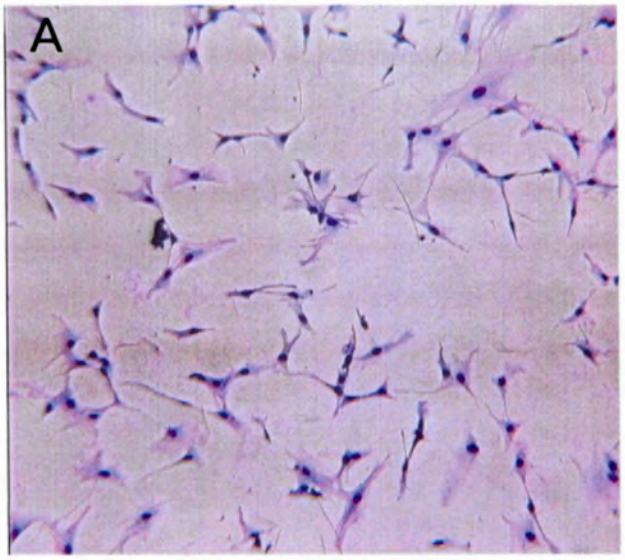

Ctrl 40 p5 1/28/99

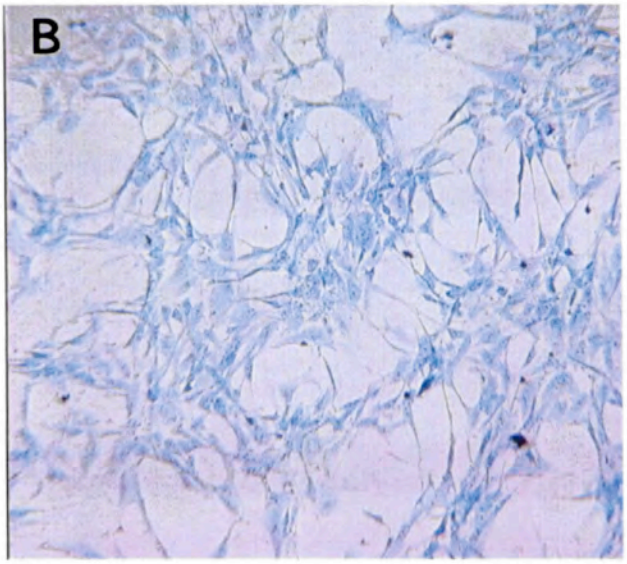

Ctrl 36 p5 1/29/99

Figure 4.6. Examples of the impacts of cell densities on T_{pot} measured

The first picture (A) was taken on 3rd day after cells were passaged, when the cell density was low and T_{pot} measured was 13 hours. The other picture (B) was taken on the fifth day and there was less space for cells to grow. As a result, the measured T_{pot} was 23 hours.

4.6A), and 23 hours on the fifth day (Figure 4.6B). T_{pot} values measured from different normal cell isolates showed very consistent results (Appendix A). The dots and error bars in Figure 4.5 represent the means and standard deviations of T_{pot} values from different normal cell isolates. To incorporate the T_{pot} values measured into the model as the cell division rate, a nonlinear regression calculated by SigmaPlot® was used to predict the relation between T_{pot} (h) and time after cells were passaged (h),

$$T_{pot} = 12.4 + 0.0913 \cdot e^{0.0432 \cdot time} \qquad (4.1)$$

This regression had a standard error of the estimate equal to 1.75 h. The standard error of the estimate ($S_{Y|X}$) is defined as,

$$S_{Y|X} = \frac{1}{n-3}\sum_{i=1}^{n}(Y_i - \hat{Y}_i)^2 \qquad (4.2)$$

where Y_i and $\hat{Y}_i$ are the observed and predicted values, respectively, and n is the sample size (Kleinbaum *et al.*, 1998). The range of values representing the underlying population generally falls within two standard errors of the observed sample mean (SPSS Inc., 1997).

4.5 Cell death rates

Time course studies were used to determine cell death rates. To obtain the numbers of dead (D) cells, the total number of cells, which was

counted on a hemocytometer, were multiplied by the fraction of dead cells, which was obtained from propidium iodide staining and flow cytometric analysis (Section 3.4). The cell death rate (β) was assumed to be constant within each passage and was defined as the value that made the following two equations having the best fit to the experimental data of normal (N) and dead (D) cells.

$$\frac{dN(t)}{dt} = N(t)\cdot[\alpha(t) - \beta] \qquad (4.3)$$

$$\frac{dD(t)}{dt} = N(t)\cdot\beta \qquad (4.4)$$

where α is the cell division rate. α is a variable and was obtained from Equations 3.1 and 4.1 (Section 4.4).

A computer program was written in MATLAB® (Appendix B) to optimize the death rate, β. The optimization was achieved by minimization of the objective function,

$$Objective\ Function = \sum\left[\frac{(predicted - observed)^2}{(observed)^{\omega}}\right] \qquad (4.5)$$

where ω is the heteroscedasticity parameter. In this optimization, $\omega = 2$ was used to represent relative weighting.

The mean cell death rate was calculated as $2.95 \times 10^{-4} \pm 6.36 \times 10^{-5}$ (h^{-1}). This is approximately equal to 1% of the average value of division rates. No significant differences were observed between the cell death rates of control and arsenic-treated cell lines.

4.6 Biologically-based dose-response (BBDR) model of the growth of SHE cells within one passage

A BBDR model for the growth of SHE cells was developed after cell division and death rates were measured. For normal SHE cells, Equation 1.1 was applied into the model with the senescence rate (γ) set equal to zero for early passages, which gives the simplified relation,

$$\frac{dN(t)}{dt} = N(t) \cdot [\alpha(t) - \beta] \qquad (4.3)$$

where N denotes the number of normal cells, and α and β are the cell division and death rates, respectively. The measurement of cell division rate was discussed in section 4.4, and death rate in section 4.5. Since only normal and senescent stages will be discussed here, the subscript one in Equation 1.1 will be ignored.

After every cell passage, there was a lag time in culture before cell division started. In the meantime, the cells spread out and adapted to the new environment. The lag time (T_{lag}) defined in this thesis is only for

modeling purposes; the mechanism of the lag phase was not studied here. The cell numbers were assumed to be unchanged during the lag time, and controlled by the division and death rates measured after T_{lag}. Cell counts from the third, fourth, and fifth days after cells were passaged were used to determine the value of T_{lag}. The starting time of the integration of Equation 4.3 which fitted the data best was determined to be T_{lag}. The optimization of T_{lag} was achieved by a computer program (Appendix C) written in MATLAB® which minimized the objective function (Equation 4.5) between the integration (predicted) and cell counts (observed).

The lag time was determined to be 41.9 hours, and the result of modeling output versus data is shown in Figure 4.7. The cell numbers remained unchanged between zero and 41.9 hours, followed by a fast growing phase. As cell density increased, the cells grew at a lower rate due to the decreasing of space. The end point of this model was the time the next passage proceeded (seven days).

4.7 BBDR model of the growth of SHE cells through the life span

To apply the model to more than one passage, the dilution we made in each passage should be taken into account. The cell number used to verify the model ($N_{corrected}$) was calculated as the cell number counted while cells being passaged (N_{count}) multiplied by the dilution factor at previous passage,

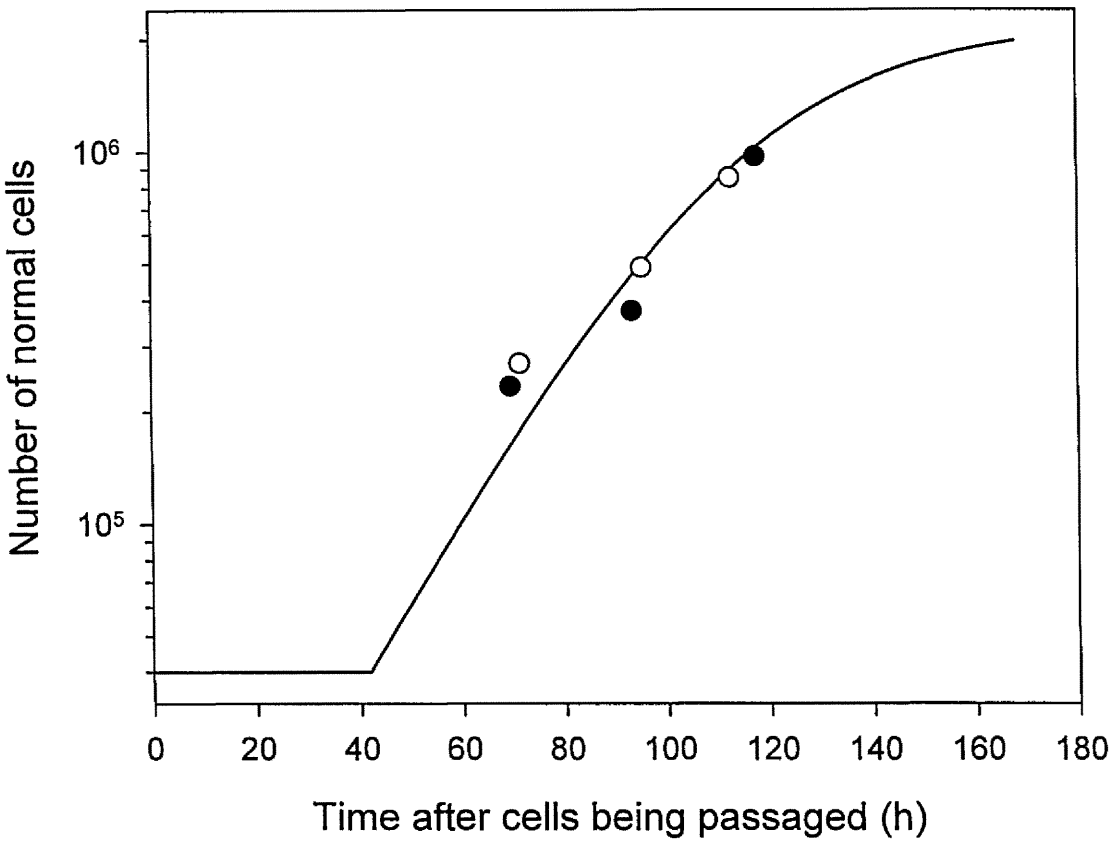

Figure 4.7. BBDR modeling of the growth of SHE cells within one passage

The *line* represents the modeling output of differential equation $dN(t)/dt = N(t) \times [\alpha(t)-\beta]$ (Appendix C) with 41.9 hours of lag time (T_{lag}). The *dots* represent the normal cell counts from the third, fourth, and fifth days after cells were passaged.

i.e. using the equation,

$$N_{corrected,i} = N_{count,i} \times \frac{N_{corrected,i-1}}{4 \times 10^4} \qquad (4.6)$$

where the value in denominator, 4×10^4, is the cell number at the beginning of every passage. The integration of Equation 4.3 was used repeatedly for all passages, while the initial number of cells of each passage was equal to the last value of previous passage (Appendix D). The result of BBDR modeling output versus experiment data is shown in Figure 4.8. These cells had been treated by arsenic for 2 days at graded concentrations, *i.e.* ●, control; ❐, 0.5 μM; ▼, 1.0 μM; ○, 2.0 μM; ◊, 5.4 μM. As is the case with a single passage (Figure 4.7), there is a lag phase in the beginning of each passage, followed by a fast growing phase with low cell density. With the increasing of cell numbers, cells grew at a lower rate. Cells were passaged weekly and another lag phase started at this point.

To further verify if the ability of arsenic to inhibit the growth of SHE cells, the standard error of estimating T_{pot} (Section 4.4) should be considered in the model. In other words, there is no significant difference among the growth of cell lines if their corrected cell numbers fall in the area between two lines which formed by the integration of Equation 4.3 with cell division rates calculated from $T_{pot} \pm 1.75$ (h). The result in Figure 4.9 indicated that there is no significant difference in growth between the cell lines treated with

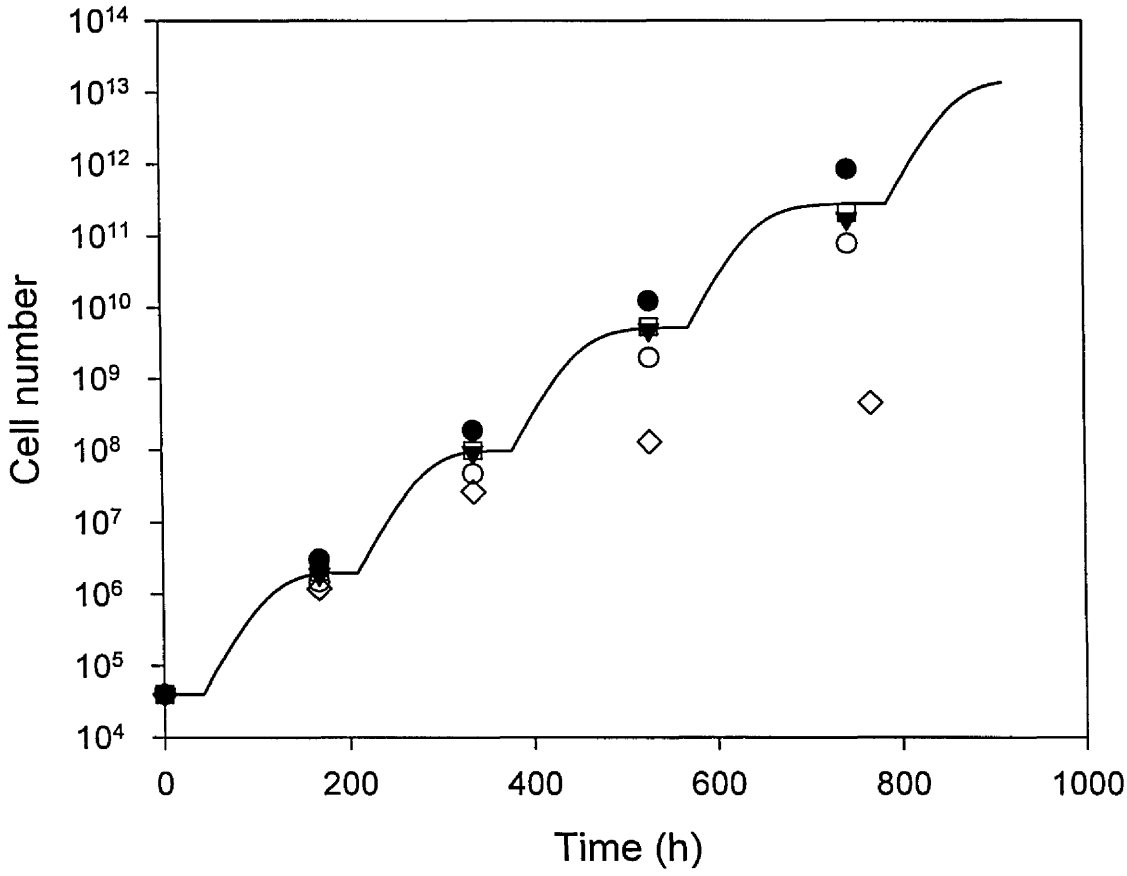

Figure 4.8. BBDR modeling of the growth of SHE cells through the life span

The *line* represents the modeling output where the integration of Equation 4.3 was used repeatedly in every passage. The *symbols* represent the corrected cell numbers where the dilution factor at each passage was taken into account. These cells had been treated by arsenic for two days at graded concentrations, *i.e.* ●, control; ❐, 0.5 μM; ▼, 1.0 μM; ○, 2.0 μM; ◇, 5.4 μM.

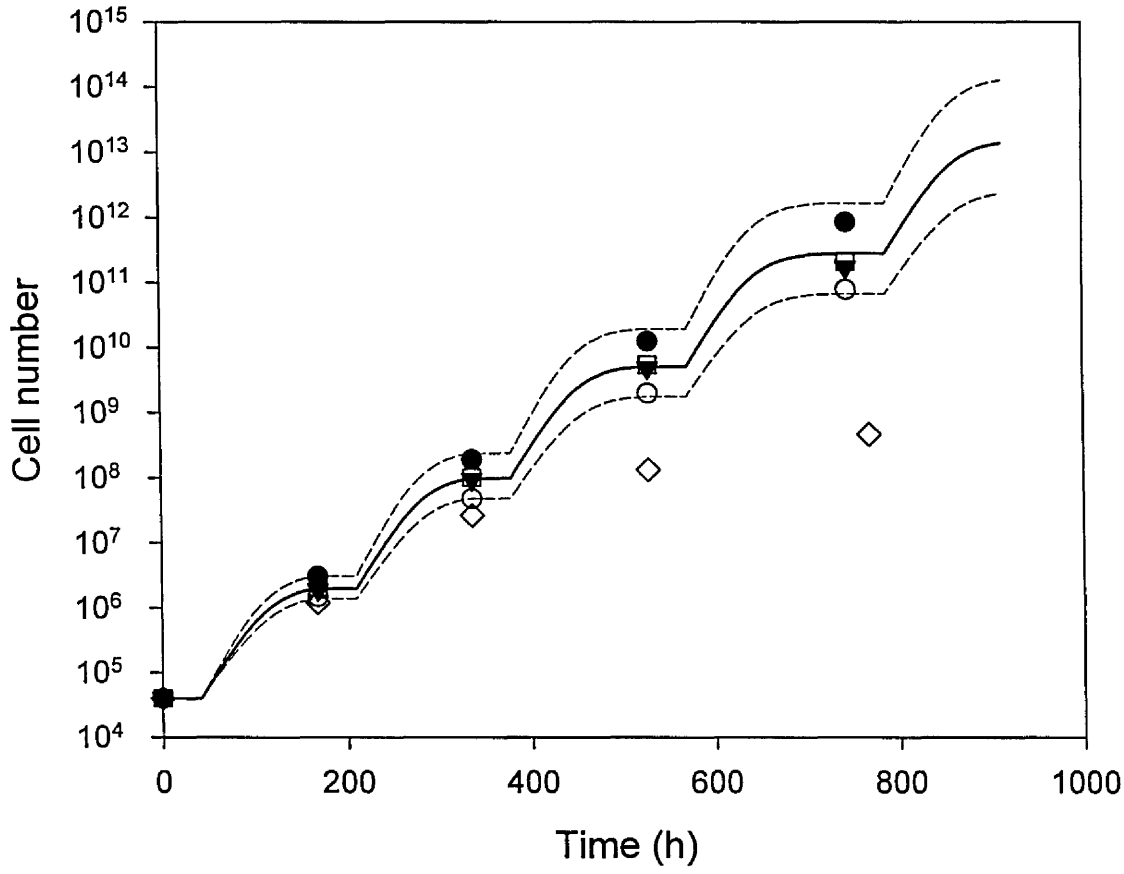

Figure 4.9. BBDR modeling of the growth of SHE cells with the standard error of estimating T_{pot} taken into account

The *solid line* represents the modeling of SHE cell growth with cell division rate calculated from Equation 4.1. The *dashed lines* reflect the uncertainty of the model based on the T_{pot} standard error (1.75 h). The *symbols* represent the corrected cell numbers of cells exposed to arsenic for two days at graded concentrations, *i.e.* ●, control; ❐, 0.5 μM; ▼, 1.0 μM; ○, 2.0 μM; ◇, 5.4 μM.

three low concentrations of arsenic and control cells. As we expected from the discussion in Section 4.3, SHE cells exposed to 5.4 μM of arsenic showed a significant inhibition of cell growth at the third and fourth passages. This cell line stop growing at the fourth passage. This gave us the information required for determining the cell senescence rate.

It was also calculated by a computer program (Appendix E) that when the means of T_{pot} values multiplied by a factor of 0.93, the resulting model output fitted the control cell counts (● in Figure 4.9) best.

4.8 The estimation of senescence rates

The potential doubling times measured from the third and fourth passages of cells exposed 5.4 μM of arsenic were much higher than from the normal cells, which is the result of increases of senescent cells. These potential doubling times incorporated with the data collected from the growth of normal cells provided the information for estimating cell senescence rates. The senescence rate was assumed to be zero, prior to the third passage of this cell line.

4.8.a The correlation between senescence rates and potential doubling times

The potential doubling time measured reflected the growth of a population containing both normal and senescent cells. Thus the more

senescent cells existed in the population, the higher the T_{pot}. Base on this result and the observation from Figure 4.9, *i.e.* a significant inhibition of cell growth was observed at the third and fourth passages in this cell line, we concluded that cells exposed to 5.4 μM of arsenic started to become senescent at the third passage and continued the process at the fourth passage where all cells stopped growing.

To calculate the number of senescent cells, Equation 1.3 was recalled and Equation 1.1 was rewritten as,

$$\frac{dN(t)}{dt} = N(t)\cdot[\alpha_{normal}(t) - \beta] - \gamma(t)\cdot N(t) \qquad (4.7)$$

$$\frac{dS(t)}{dt} = \gamma(t)\cdot N(t) \qquad (1.3)$$

where N and S denote the number of normal and senescent cells, respectively, and α, β, and γ denote the cell division, death, and senescence rates, respectively. The cell death rate, β, was calculated in Section 4.5 and assumed to be constant. Cell division rate with subscript normal is the rate we discussed in Section 4.4. The division rate of normal cell (α_{normal}) should be distinguished from the division rates measured at the third and fourth passages of the cells exposed to 5.4 μM of arsenic, α_{mix}, which is the rate of a mixed population of normal and senescent cells. Since α_{mix} reflected the

growth of the mixed population, we should discuss it from the summation of Equations 4.7 and 1.3, *i.e.*

$$\frac{d[N(t)+S(t)]}{dt} = N(t)\cdot\alpha_{normal}(t) - N(t)\cdot\beta \qquad (4.8)$$

Since the potential doubling time, which was used to calculated cell division rate, was defined as a cell cycling time that takes growth fraction but not cell loss into account, Equation 4.8 was rewritten as,

$$\frac{d[N(t)+S(t)]}{dt} = [N(t)+S(t)]\cdot\alpha_{mix}(t) - N(t)\cdot\beta \qquad (4.9)$$

From Equation 4.8 and 4.9, the fraction of the normal cells in the mixed population was calculated as,

$$\frac{N(t)}{N(t)+S(t)} = \frac{\alpha_{mix}(t)}{\alpha_{normal}(t)} \qquad (4.10)$$

By incorporating Equation 3.1 into this equation, it could be rewritten as,

$$\frac{N(t)}{N(t)+S(t)} = \frac{T_{pot_{normal}}(t)}{T_{pot_{mix}}(t)} \qquad (4.11)$$

According to our assumption that cells exposed to 5.4 μM of arsenic were in the process of becoming senescent at the third and fourth passages, cell

numbers counted in these passages were considered as the total number of normal and senescent cells, *i.e.* N(t) + S(t). Thus the numbers of normal as well as senescent cells at these two passages were calculated from Equation 4.10 and cell counts.

4.8.b The correction of the potential doubling time according to crowding factor

While using T_{pot} values measured at the third and fourth passages to calculate the senescence rates, T_{pot} values were corrected according to the "crowding" factor because T_{pot} values are affected by both the "senescent" and "crowding" factors at these two passages. To correct the crowding factor, the change of T_{pot} as a function of cell number per plate is shown in Figure 4.10. The cell numbers were calculated by the same program used to predict the of growth of cells within one passage as shown in Figure 4.7. The division rates were calculated by means of T_{pot} values (Equation 4.1) multiplied by a factor of 0.93 to obtain the best fit to control cells (Section 4.7).

Whether the senescent cell populations had great impact on the T_{pot} values was verified by normalizing the T_{pot} values by the T_{pot} values measured at the third day after the cells were passaged (Figure 4.11). The normalized T_{pot} values provided information about the change of T_{pot} values within each

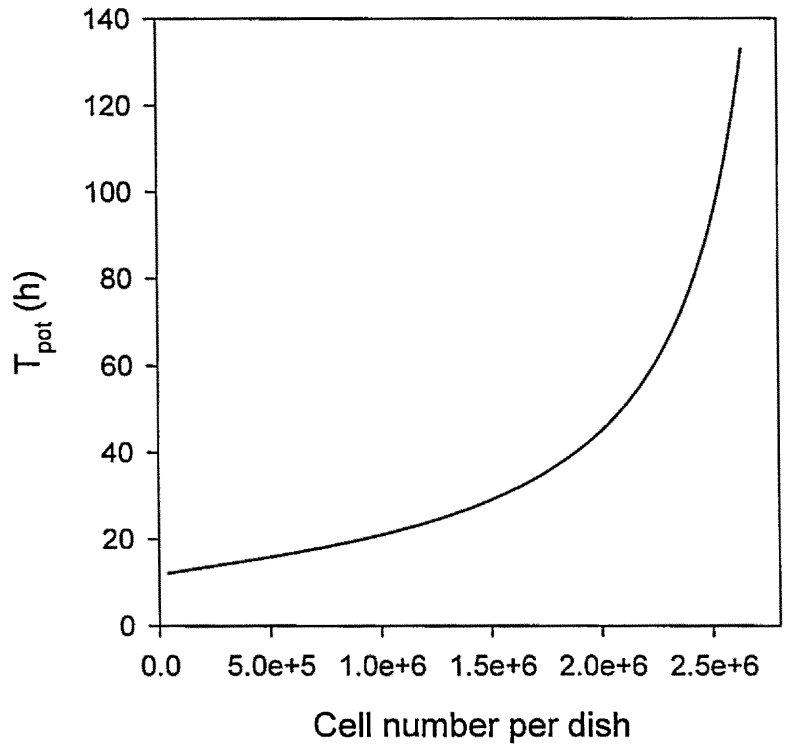

Figure 4.10. The change of potential doubling time (T_{pot}) as a function of cell density

The means of T_{pot}s (Equation 4.1) multiplied by a factor of 0.93 was used to calculate the division rates (α) in the equation, $dN(t)/dt = N(t) \times [\alpha(t)-\beta]$, which was used to calculate the cell number in each dish.

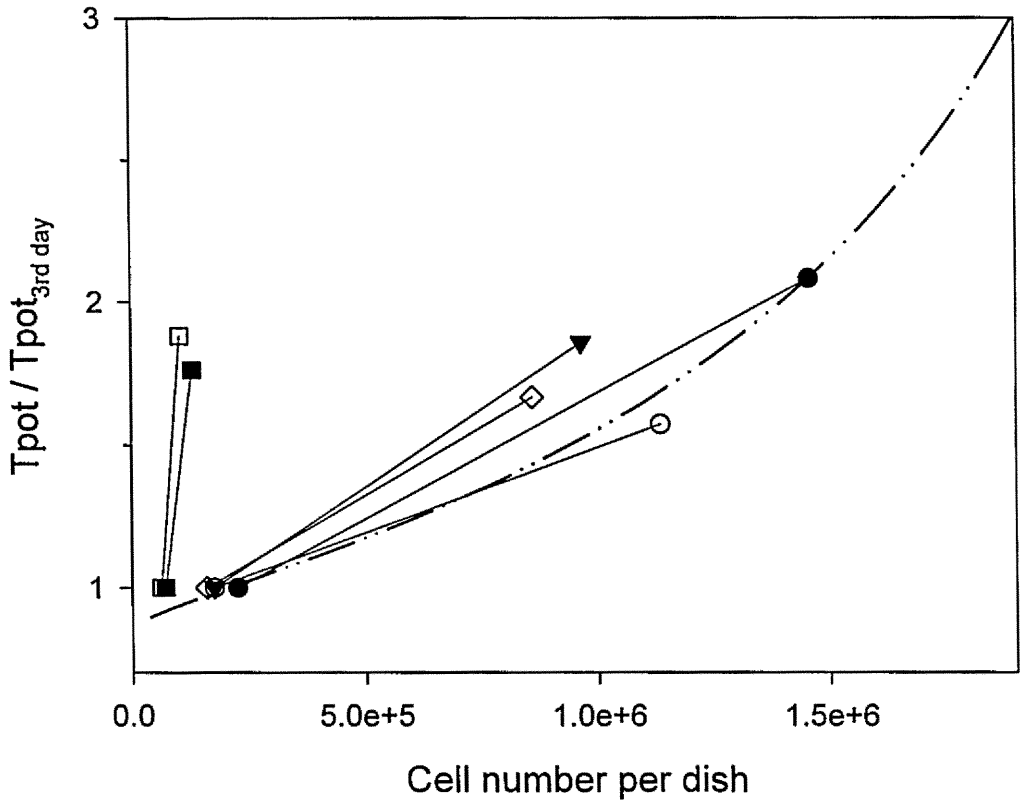

Figure 4.11. The effect of senescent cell population on potential doubling time (T_{pot}).

Potential doubling times were normalized according to the value measured at the third day after passage in each cell line. The *dashed-dot line* represents the standard curve which only reflected the crowding factor on normalized T_{pot} and was normalized from Figure 4.10. The *symbols*, ●, ○, ▼, and ◊ represent the normalized T_{pot}s of control cells and cells exposed to the three lower concentration of As (0.5, 1.0, and 2.0 μM), respectively.

passage, with all data presented on a comparable scale. The standard curve, which represented a function that the change of T_{pot} values was only related to the crowding factor (dashed-dot line in Figure 4.11), was normalized from Figure 4.10. In all samples shown in Figure 4.11, T_{pot} values were only measured on the third and fifth days after cell passage.

The changes of the normalized T_{pot} values in control cells and cells exposed to the three lower concentration of arsenic (●, ○, ▼, and ◊ in Figure 4.11) all followed the same pattern the standard curve had, which suggested their T_{pot} values were only affected by cell densities. For cells exposed to 5.4 μM of arsenic, the normalized T_{pot} values increased 1.76 and 1.88 folds at third and fourth passages in a time span of 2 days, but with only slight increases in the cell numbers. The normalized T_{pot} values of standard curve only increased 1.04 folds with the same amount of change in the cell numbers. These results suggested that the senescent cells in the population slowed the growth of the whole population.

4.8.c The prediction of the growth of a cell population including normal and senescent cells

For a cell population including both normal and senescent cells, the cell growth was much slower than for a population consisting only of normal cells. Therefore, the cell division rates calculated in Section 4.4 could not be

used here, *i.e.* the cell division rates applied to Equation 4.9 should be estimated separately. It was assumed that the changes of T_{pot} values with time of these mixed population followed the same pattern the normal cells had. Three parameters exponential equations similar to Equation 4.1 ($T_{pot} = y_0 + a \cdot e^{b \cdot time}$; y_0, a, b are constants) can be used to fit the data of T_{pot} values versus time after passages. Available data for the mixed population cells were the T_{pot} values and cell numbers from third and fourth passages of the cells exposed to 5.4 μM of arsenic. Two T_{pot} values, at 72 and 120 hours after cells being passaged, from each of these two passages were measured. Since at least three data points were needed for the three parameters exponential equation, the cell number counted in the end of the passage was incorporated to the data fitting of T_{pot}. The cell growth was simulated by a computer program (Appendix F) which first fitted the distribution of T_{pot} values with the three parameters exponential equation by finding the T_{pot} in the end of the passage, *i.e.* the T_{pot} resulting the calculated cell number fitted the experimental data best. The modeling predictions, which using the integration of Equation 4.9, of the cell growth of the mixed cell populations are shown in Figure 4.12.

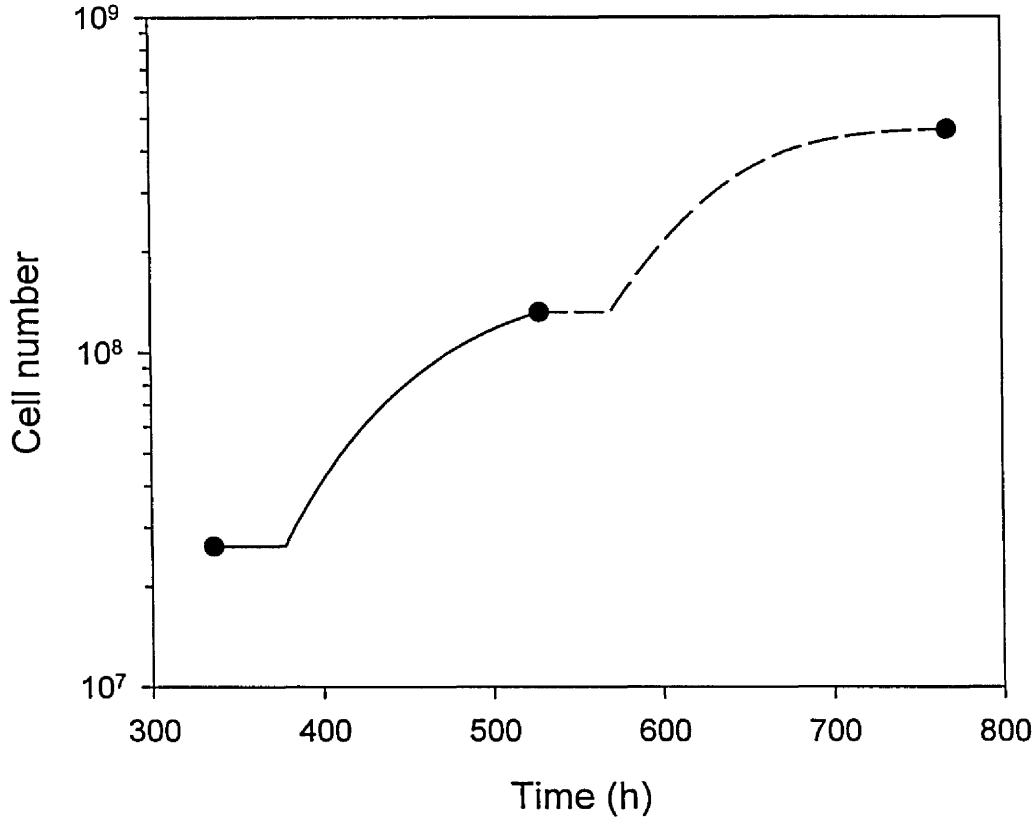

Figure 4.12. The prediction of the growth of a cell population including both normal and senescent cells

The *solid* and *dashed line* represent the modeling predictions of the growth of the cells exposed to 5.4 μM of As at the third and fourth passages, respectively. The *dots* represent the experimental data of cell numbers from this cell line. The T_{pot}s used in this model was optimized by the computer program as shown in Appendix F, with the results that
$T_{pot} = 0.843 + 17.4 * e^{0.0120 * t}$ for the third passage and
$T_{pot} = 31.8 + 2.89 * e^{0.0256 * t}$ for the fourth passage.

4.8.d The optimization of cell senescence rate

The senescence rates (γ) was defined as the values that result in the best predictions of the number of senescent cells (S) (calculated from Equation 1.3) and normal cells (N) (calculated from Equation 4.7). The predicted numbers of senescent cells were verified by the experimental data calculated from Equation 4.11, whereas the summation of predicted normal and senescent cells were verified by the data calculated from Equation 4.9.

The optimization of the cell senescence rates was achieved by a program (Appendix G) executed by ACSL. The results of optimization are shown in Figure 4.13 where the values between 336 and 528 hours represent the cell growth of the third passage of the cells exposed to 5.4 μM of arsenic and those between 528 and 768 hours represent the fourth passage. The senescence rates estimated was 0.0543 h^{-1} for the third passage and 0.057 h^{-1} for the fourth passage. The *solid line* and *solid circles* denote the experimental data of total and senescent cells, respectively. The predicted values of normal (from Equation 4.7), senescent (from Equation 1.3), and total cells (the summation of previous two numbers) are expressed by the *dot*, *dashed*, and *dashed-dot lines*, respectively. Most of the predicted numbers of senescent cells (dashed line) were higher than the experimental data (dots). The predicted numbers of total cells (dashed-dot line) were higher than experimental data (solid line) at the third passage and

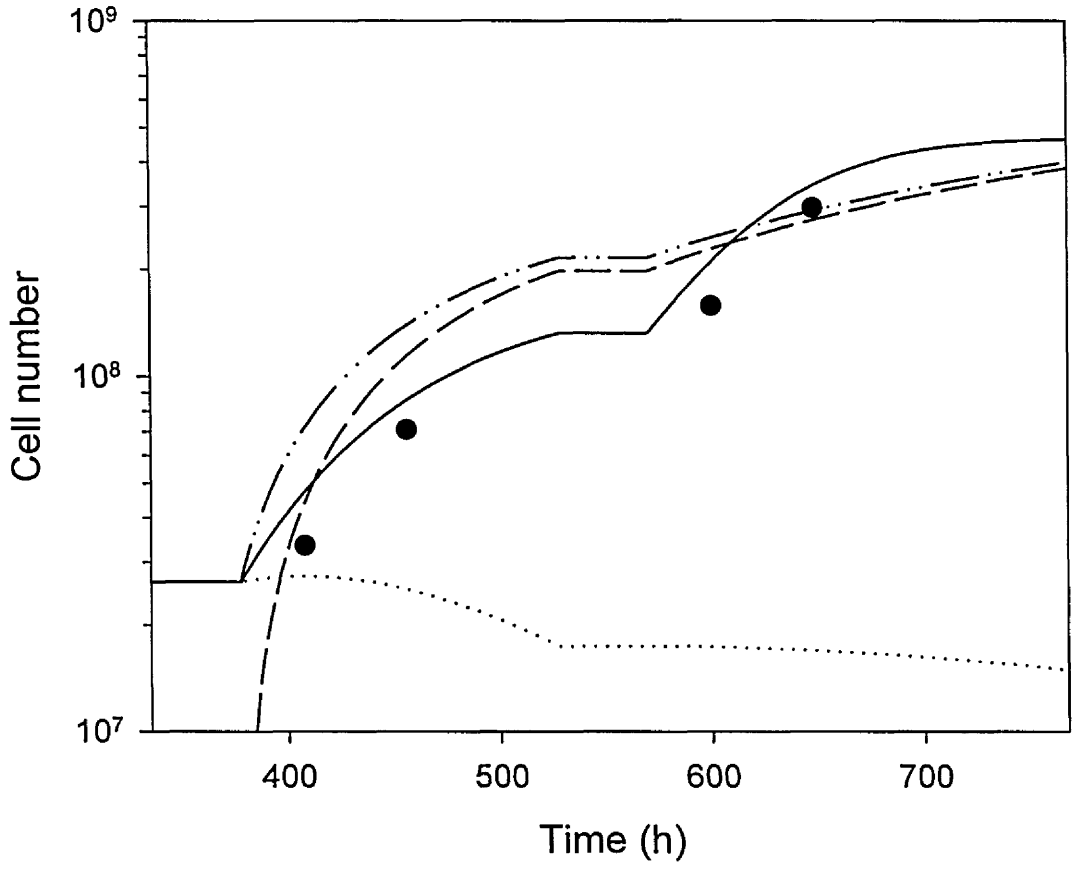

Figure 4.13. The estimation of cell senescence rate

the values between 336 and 528 hours represent the cell growth of the third passage of the cells exposed to 5.4 μM of arsenic and those between 528 and 768 hours represent the fourth passage. The *solid line* and *solid circles* denote the experimental data of total and senescent cells, respectively. The predicted values of normal, senescent, and total cells are expressed by the *dot*, *dashed*, and *dashed-dot lines*, respectively. The estimated senescence rates were 0.0543 h^{-1} for the third passage and 0.057 h^{-1} for the fourth passage.

lower at the fourth passages.

The deviation of the predicted values from experimental data was assumed to be caused by the overestimated division rates of normal cells. A high senescence rate was obtained at third passage in order to compensate the overestimated division rate. The high senescence rate meant more normal cells becoming senescent cells, which resulting in the extremely low number of normal cells in the end of the third passage, *i.e.* in the beginning of the fourth passage. Since only the normal cells proliferated and the initial value was low, the total cell number was not able to match the experimental data in the fourth passage.

The assumption that the division rates of normal cells were overestimated was based on the observation that the senescent cells were much larger than the normal cells (Figure 4.3). Since the senescent cells occupied much larger areas than the normal cells did, *i.e.* normal cells grew slower in the mixed population than we estimated, the crowding factor for estimating cell division rates should be modified. It was estimated from a program written in ACSL (Appendix H) that the division rates of the normal cells should be multiplied by a factor of 0.34 to correct the crowding effect. The senescence rates were estimated as 0.0103 h^{-1} for the third passage and 0.0175 h^{-1} for the fourth passage (Figure 4.14) with the corrected normal cell division rates. The model made very good predictions of the total cell

numbers. Unlike the results in Figure 4.13, the predicted cell numbers followed the same growth pattern the experimental data had at both the third and fourth passages in Figure 4.14. Although the prediction of senescent cell numbers were not as good as of the total cell number, the experimental data of total cell numbers, which were obtained directly from the counting, were more reliable than the data of senescent cell numbers calculated by the ratio of potential doubling times. The modeling predictions of the growth of the cells in mixed population was incorporated the predictions for normal cells and is shown in Figure 4.15.

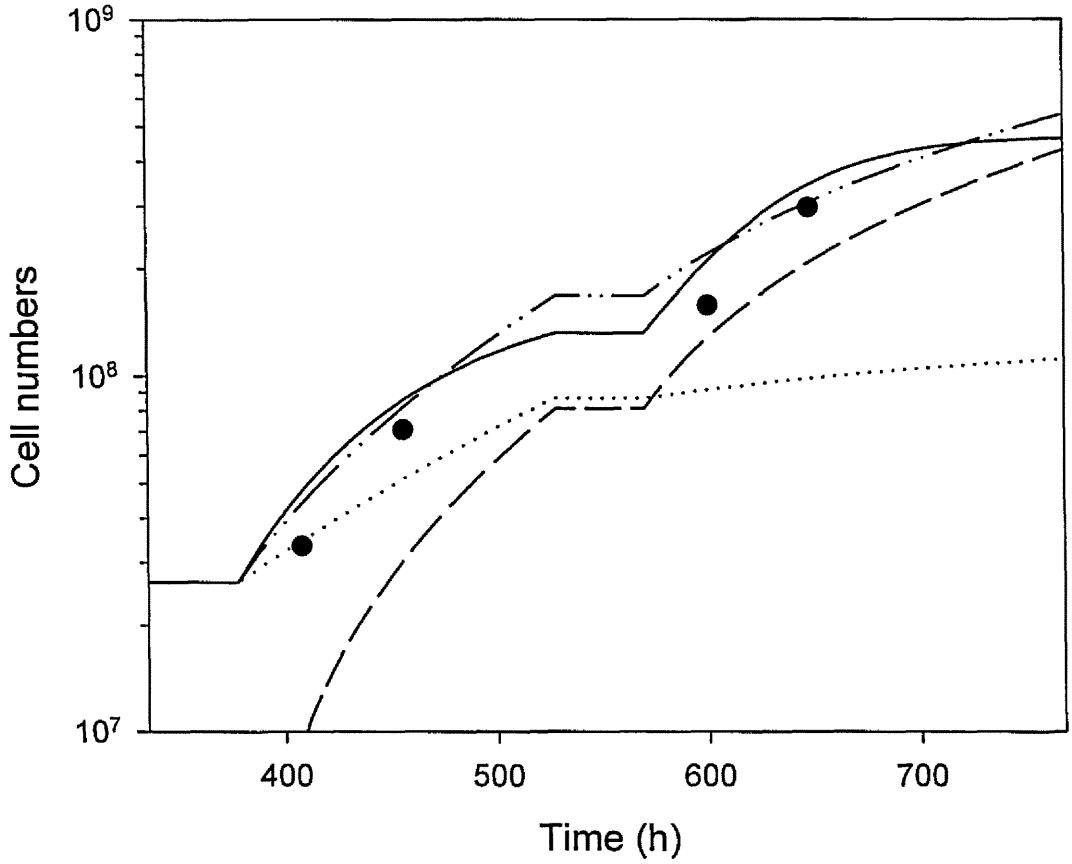

Figure 4.14. The estimation of senescence rates with corrected normal cell division rates

The normal cell division rates were multiplied by a factor of 0.34 to correct the crowding effect due to the different sizes of senescent and normal cells. Cell senescence rates were estimated as 0.0103 h^{-1} at the third passage and 0.0175 h^{-1} at the fourth passage. As in Figure 4.13, the *solid line* and *solid circles* denote the experimental data of total and senescent cells, respectively. The predicted values of normal, senescent, and total cells are expressed by the *dot*, *dashed*, and *dashed-dot lines*, respectively.

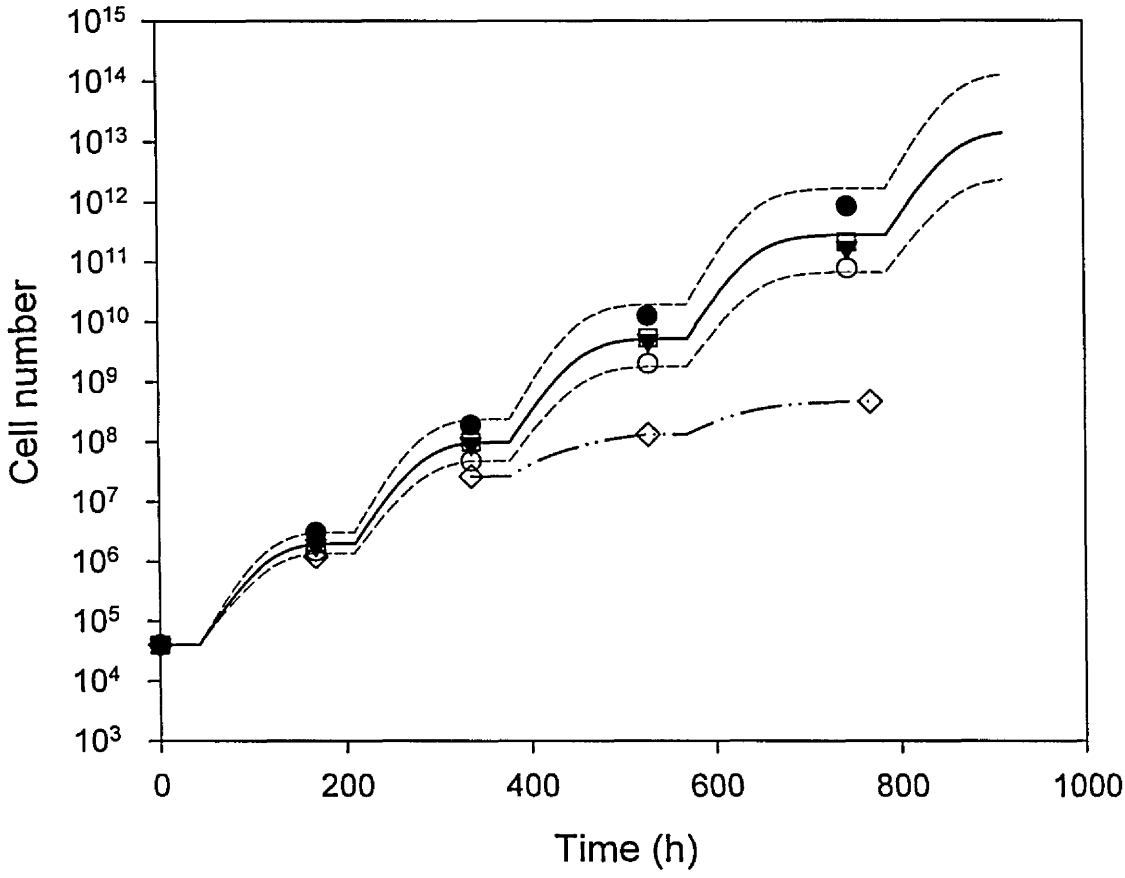

Figure 4.15. The modeling predictions of the growth of normal cells and cells in the population including both normal and senescent cells

The *solid line* represents the modeling predictions of the growth of normal SHE cells. The *dashed lines* reflect the uncertainty of the model based on the T_{pot} standard error. The *dashed-dot line* represents the predictions of the growth of the cells in a mixed population including normal and senescent cells The *symbols* represent the cell numbers of cells exposed to arsenic for two days at graded concentrations, *i.e.* ●, control; ❐, 0.5 μM; ▼, 1.0 μM; ○, 2.0 μM; ◇, 5.4 μM.

CHAPTER 5

Conclusions

The biologically-based dose-response model developed in our laboratory was proven to predict the growth of normal Syrian hamster embryo (SHE) cells successfully. The model was biologically-based since the cell division and death rates applied in the model were measured by flow cytometry, and the cell numbers calculated by the model were consistent with the experimental data. The flow cytometric methods used in here could be applied to other cell lines easily for modeling purpose.

Results from cytotoxicity studies show that a mixture of the three metals (arsenic, chromium, and lead) are less-than-additive, suggesting antagonistic interaction at the level of cell killing. No immortal cell line was observed after serial passages of the cells exposed to the LC_{50} of the three metals individually and as a mixture.

For normal SHE cells, the cell division rates decreased as cell densities increased due to the shortage of space for cell growth. The potential doubling times, which were directly measured by flow cytometry and used to calculated division rate, ranged from 12 to 59 hours, depending on the degree of confluence of cell cultures. As a result, a fast growth phase

followed the lag phase (Figure 4.9) and the cell growth slowed down as cell numbers increased. The cells were passaged once a week and another cycle followed the same growth pattern began then. The cell death rates we measured were much smaller than the division rate, which was a result expected under exponential growth conditions.

SHE cells exposed for two days to 5.4 μM of arsenic, which was the LC_{50} of arsenic to SHE cells analyzed by MTT assays, expressed growth inhibition at the third and fourth passage. These cell lines only grew for 16 population doublings before becoming senescent, while control cells and those exposed to lower concentrations of arsenic grew for at least 30 population doublings. The cells exposed to lower concentrations, 0.5, 1.0, and 2.0 μM, of arsenic did not express significant differences in growth rates from control cells.

Cell senescence rates were estimated from the experimental data generated from the cells exposed to 5.4 μM of arsenic. This cell line grew much more slowly than the control cell line during the third and fourth passages. This decreased growth rate was caused by the increase of senescent cells in the population. While estimating the senescence rate, the division rate of normal cells should be multiplied by a factor of 0.34 to correct the crowding effect due to the different sizes in normal and senescent cells. The senescence rates were measured as 0.0103 and

0.0175 h^{-1} for the third and fourth passages, respectively (Figure 4.14).

Mechanisms responsible for induction of cellular senescence in SHE cells exposed to arsenic may be involved in the apparent inability of arsenic to induce neoplasia in experimental animals. The genetic changes associated with arsenic-induced senescence *in vitro* may be related to the absence of tumor development in test animals. In combination with an appropriate human *in vitro* system, the SHE cell system could serve as a tool for comparing differences in carcinogenic mechanisms of arsenic between laboratory animals and humans.

CHAPTER 6

Future Directions

All the techniques for measuring cell division and death rates developed in our laboratory could be applied to other cell lines for modeling purposes. The model has the potential to be applied to *in vitro* human cell lines, and further incorporate their *in vivo* counterpart with physiological-based pharmacokinetic/pharmacodynamic modeling for risk assessment.

With the successful prediction of the growth of Syrian hamster embryo (SHE) cells, it is worthwhile to improve the experimental system. The first improvement is to passage cells every five days instead seven days. Since the cell growth is strongly dependent on the crowding effect on the culture plate, a shorter period between each passage could reduce the impact of cell density on cell division rates. For example, the data in Figure 4.4 imply that a 5-day passage frequency would be adequate, since the cells still grew at relative high rate at the fifth day before the crowding effect had strong impact on the growth. Furthermore, the consistency of the assay can be improved by quantifying the ratio of metabolizing to transformable cell types in the initial cell population.

Improvements also could be made to better estimate the cell senescence rates. In our experiments, we successfully predicted of total cell numbers with adjusted normal cell division rates, but the senescent cell numbers predicted were lower than the experimental data (Figure 4.13). In order to obtain more information for estimating the cell senescence rates, potential doubling times should be measured every day instead of the third and fifth days after cells start the process of becoming senescent.

There was a lag phase, in which the cell numbers stayed unchanged, in the beginning of each passage in our model. This lag phase was actually a undetermined area where insufficient amount of cells were accumulated for flow cytometric analysis. To study the detail of the behavior of cells in this time period, the experiment should start with a large amount of cells in every passage. As a result, culture plates with larger area should be used to compensate the crowding effect caused by the increased initial cell numbers.

To further study the abilities of the chemicals chosen in this thesis to induce neoplastic transformations in SHE cells for modeling purpose, it is worthwhile to repeat the experiments with seven day exposure instead of two day period. As soon as the cells immortal or later stages are obtained, the parameters of cell growth in each stage could be estimated and thus the quantitative cancer model will be completed.

The mutation rate μ was not estimated in the thesis due to the unavailability of immortal cell lines. Since it is an important parameter in the model, the calculation of mutation rates are discussed as follows. Fluctuation analysis proposed by Luria and Delbruck (Luria and Delbruck, 1943) were widely used to estimate cell mutation rates *in vitro* (Crawford *et al.*, 1983; Kraemer *et al.*, 1986; Bols *et al.*, 1991; Bols *et al.*, 1992; Dumontet *et al.*, 1996). The distribution of the numbers of mutation in series of similar cultures which are plated in parallel is analyzed (Luria and Delbruck, 1943). The mutation rate is then calculated as

$$\nu = \frac{(\ln 2)(-\ln P_0)}{N_f - N_0} \qquad (6.1)$$

where v is the mutations per cell per division cycle, P_0 represents the fraction of culture with no mutants, N_f and N_0 are the final and initial number of cell (Luria and Delbruck, 1943). The term (-ln P_0) in Equation 6.1 is the number of mutations per culture (m) calculated from the equation

$$P_0 = e^{-m} \qquad (6.2)$$

with the assumption that the distribution of all mutations is according to Poisson's law (Luria and Delbruck, 1943). For example, if one out of 30 colonies isolated become immortal cell line in my experiment, the fraction of culture with no immortalization occurred (P_0) is equal to 29/30 and the

number of mutation per culture (m) is 0.034.

The mutation rate estimated by fluctuation analysis can not be directly applied to the model proposed in this thesis, since the mutation rate μ_i in this model is defined as the probability of mutation that a stage i cell divides into one stage i cell and one stage i + 1 cell, *i.e.* the number of mutation per cell division. With the derivation discussed in Appendix I, the mutation rate μ in the model can be calculated as

$$\mu = \frac{-\ln P_0}{N_f - N_0} \qquad (6.3)$$

For the control cells in my experiments, isolated colonies can expand to approximately 5×10^6 cells (N_f), which is assumed to start with 1 cell (N_0), and no immortal cell lines were observed from 30 isolated colonies. Thus the spontaneously mutation rate μ_1 for normal cells become immortal cells is less than

$$\frac{-\ln(29/30)}{5 \times 10^6 - 1} = 6.8 \times 10^{-9} \text{ mutation per cell division}$$

Mutation rates have been broadly defined as mutation per cell per generation (Luria and Delbruck, 1943), mutation per viable cell (Bols, Naaktgeboren, and Simons, 1991), mutation per time unit (Moolgavkar and Knudson, Jr., 1981). With modeling purpose in SHE cell system, the

mutation rate can be estimated from Equation 6.3, a modified form of fluctuation analysis.

CHAPTER 7

References

AGENCY FOR TOXIC SUBSTANCES AND DISEASE REGISTRY (ATSDR), 1990a. *Case Studies in Environmental Medicine: Arsenic Toxicity*. Atlanta: U.S. Department of Health and Human Services, Public Health Service.

AGENCY FOR TOXIC SUBSTANCES AND DISEASE REGISTRY (ATSDR), 1990b. *Case Studies in Environmental Medicine: Chromium Toxicity*. Atlanta: U.S. Department of Health and Human Services, Public Health Service.

AGENCY FOR TOXIC SUBSTANCES AND DISEASE REGISTRY (ATSDR), 1992. *Case Studies in Environmental Medicine: Lead Toxicity*. Atlanta: U.S. Department of Health and Human Services, Public Health Service.

AGENCY FOR TOXIC SUBSTANCES AND DISEASE REGISTRY (ATSDR), 1993b. *ATSDR: Chromium*. Atlanta: U.S. Department of Health and Human Services, Public Health Service.

AGENCY FOR TOXIC SUBSTANCES AND DISEASE REGISTRY (ATSDR), 1993d. *ATSDR: Lead*. Atlanta: U.S. Department of Health and Human Services, Public Health Service.

AGENCY FOR TOXIC SUBSTANCES AND DISEASE REGISTRY (ATSDR), 1993a. *Toxicological Profile for Arsenic*. Atlanta: U.S. Department of Health and Human Services, Public Health Service.

AGENCY FOR TOXIC SUBSTANCES AND DISEASE REGISTRY (ATSDR), 1993c. *Toxicological Profile for Chromium*. Atlanta: U.S. Department of Health and Human Services, Public Health Service.

ALBERTS B, BRAY D, LEWIS J, RAFF M, ROBERTS K, WATSON JD, 1994. The Cell-Division Cycle. In: *Molecular Biology of the Cell*. New York: Garland Publishing, 863-910.

ARMITAGE P, DOLL R, 1954. The Age Distribution of Cancer and a Multi-stage Theory of Carcinogenesis. *British Journal of Cancer* 8:1-12.

ARMITAGE P, DOLL R, 1957. A Two-Stage Theory of Carcinogenesis in Relation to the Age Distribution of Human Cancer. *British Journal of Cancer* 11:161-169.

BALLANTYNE B, MARRS T, TURNER P, 1995. Fundamentals of Toxicology. In: *General and Applied Toxicology*. New York: Stockton Press, 3-38.

BANDTLOW C, ZACHLEDER T, SCHWAB ME, 1990. Oligodendrocytes Arrest Neurite Growth by Contact Inhibition. *The Journal of Neuroscience* 10:3837-3848.

BARRETT JC, 1979. The Progressive Nature of Neoplastic Transformation of Syrian Hamster Embryo Cells in Culture. *Progress in Experimental Tumor Research* 24:17-27.

BARRETT JC, 1993. Neoplastic Progression of Syrian Hamster Embryo Cells in Culture. *Proceedings of the Society for Experimental Biology and Medicine* 202:30-36.

BEGG AC, MCNALLY NJ, SHRIEVE DC, KARCHER H, 1985. A Method to Measure the Duration of DNA Synthesis and the Potential Doubling Time From a Single Sample. *Cytometry* 6:620-626.

BERWALD Y, SACHS L, 1963. *In Vitro* Cell Transformation with Chemical Carcinogens. *Nature* 200:1182-1184.

BERWALD Y, SACHS L, 1965. *In Vitro* Transformation of Normal Cells to Tumor Cells by Carcinogenic Hydrocarbons. *Journal of the National Cancer Institute* 35:641-661.

BOLS BLMC, NAAKTGEBOREN JM, LOHMAN PHM, SIMONS JWIM, 1992. Immortalization of Carcinogen-treated Syrian Hamster Embryo Cells Occurs Indirectly via an Induced Process. *Cancer Research* 52:2253-2256.

BOLS BLMC, NAAKTGEBOREN JM, SIMONS JWIM, 1991. Immortalization of Syrian Hamster Embryo Cells Is in Itself a Multistep Event. *Cancer Research* 51:1177-1184.

BOYD JA, BARRETT JC, 1990. Genetic and Cellular Basis of Multistep Carcinogenesis. *Pharmacology and Therapeutics* 46:469-486.

COHEN MD, KARGACIN B, KLEIN CB, COSTA M, 1993. Mechanisms of Chromium Carcinogenicity and Toxicity. *Critical Reviews in Toxicology* 23:255-281.

CONOLLY RB, KIMBELL JS, 1994. Computer Simulation of Cell Growth Governed by Stochastic Processes: Application to Clonal Growth Cancer Models. *Toxicology and Applied Pharmacology* 124:284-295.

COOPER GM, 1992a. Basic Facts About Cancer.In: *Elements of Human Cancer*. Boston: Jones and Bartlett Publishers, 3-14.

COOPER GM, 1992b. Cancer and the Environment.In: *Elements of Human Cancer*. Boston: Jones and Bartlett Publishers, 31-62.

COSTA M, 1997. Toxicity and Carcinogenicity of Cr(VI) in Animal Models and Humans. *Critical Reviews in Toxicology* 27:431-442.

CRAWFORD BD, BARRETT JC, TS'O POP, 1983. Neoplastic Conversion of Preneoplastic Syrian Hamster Cells: Rate Estimation by Fluctuation Analysis. *Molecular and Cellular Biology* 3:931-945.

CRUMP KS, 1996. The Linearized Multistage Model and the Future of Quantitative Risk Assessment. *Human and Experimental Toxicology* 15:787-798.

DEWANJI A, VENZON DJ, MOOLGAVKAR SH, 1989. A Stochastic Two-Stage Model for Cancer Risk Assessment. II. The Number and Size of Premalignant Clones. *Risk Analysis* 9:179-187.

DUMONTET C, DURAN GE, STEGER KA, BEKETIC-ORESKOVIC L, SIKIC BI, 1996. Resistance Mechanisms in Human Sarcoma Mutants Derived by Single-Step Exposure to Paclitaxel (Taxol). *Cancer Research* 56:1091-1097.

GILMER TM, ANNAB LA, BARRETT JC, 1988. Characterization of Activated Proto-Oncogenes in Chemically Transformed Syrian Hamster Embryo Cells. *Molecular Carcinogenesis* 1:180-188.

HAO Y, CRENSHAW T, MOULTON T, NEWCOMB E, TYCKO B, 1993. Tumour-Suppressor Activity of *H19* RNA. *Nature* 365:764-767.

JOLLIFFE DM, 1993. A History of the Use of Arsenicals in Man. *Journal of the Royal Society of Medicine* 86:287-289.

KANISAWA M, SCHROEDER HA, 1967. Life Term Studies on the Effects of Arsenic, Germanium, Tin, Vanadium on Spontaneous Tumors in Mice. *Cancer Research* 27:1192-1195.

KLEINBAUM DG, KUPPER LL, MULLER KE, NIZAM A, 1998. *Applied Regression Analysis and Other Multivariable Methods*.Pacific Grove: Duxbury Press, 51-52.

KOI M, AFSHARI CA, ANNAB LA, BARRETT JC, 1989. Role of a Tumor-Suppressor Gene in the Negative Control of Anchorage-Independent Growth of Syrian Hamster Cells. *Proceedings of the National Academy of Sciences of the United States of America* 86:8773-8777.

KOI M, BARRETT JC, 1986. Loss of Tumor-Suppressive Function during Chemically Induced Neoplastic Progression of Syrian Hamster Embryo Cells. *Proceedings of the National Academy of Sciences of the United States of America* 83:5992-5996.

KRAEMER PM, RAY FA, BROTHMAN AR, BARTHOLDI MF, CRAM LS, 1986. Spontaneous Immortalization Rate of Cultured Chinese Hamster Cells. *Journal of the National Cancer Institute* 76:703-709.

LARSEN JK, 1994. Measurement of Cytoplasmic and Nuclear Antigens.In: Ormerod MG, ed. *Flow Cytometry: A Practical Approach*. Oxford: Oirl Press, 93-117.

LEBOEUF RA, KERCKAERT GA, 1986. The Induction of Transformed-like Morphology and Enhanced Growth in Syrian Hamster Embryo Cells Grown at Acidic pH. *Carcinogenesis* 7:1431-1440.

LEBOEUF RA, KERCKAERT GA, AARDEMA MJ, GIBSON DP, 1990. Multistage Neoplastic Transformation of Syrian Hamster Embryo Cells Cultured at pH 6.70. *Cancer Research* 50:3722-3729.

LEBOEUF RA, KERCKAERT GA, POILEY JA, RAINERI R, 1989. An Interlaboratory Comparison of Enhanced Morphological Transformation of Syrian Hamster Embryo Cells Cultured under Conditions of Reduced Bicarbonate Concentration and pH. *Mutation Research* 222:205-218.

LEE TC, LEE KCC, CHANG C, JWO WL, 1986. Cell-Cycle Dependence of the Cytotoxicity and Clastogenicity of Sodium Arsenite in Chinese Hamster Ovary Cells. *Bulletin of the Institute of Zoology, Academia Sinica* 25:91-97.

LURIA SE, DELBRUCK M, 1943. Mutations of Bacteria from Virus Sensitivity to Virus Resistance. *Genetics* 28:491-511.

MOOLGAVKAR SH, 1979. Two-Event Models for Carcinogenesis: Incidence Curves for Childhood and Adult Tumors. *Mathematical Biosciences* 47:55-77.

MOOLGAVKAR SH, 1983. Model for Human Carcinogenesis: Action of Environmental Agents. *Envirnomental Health Perspectives* 50:285-291.

MOOLGAVKAR SH, DAY NE, STEVENS RG, 1980. Two-Stage Model for Carcinogenesis: Epidemiology of Breast Cancer in Females. *Journal of the National Cancer Institute* 65:559-569.

MOOLGAVKAR SH, DEWANJI A, VENZON DJ, 1988. A Stochastic Two-Stage Model for Cancer Risk Assessment. I. The Hazard Function and the Probability of Tumor. *Risk Analysis* 8:383-392.

MOOLGAVKAR SH, KNUDSON AG, JR., 1981. Mutation and Cancer: A Model for Human Carcinogenesis. *Journal of the National Cancer Institute* 66:1037-1052.

MORTON WE, DUNNETTE DA, 1994. Health Effects of Environmental Arsenic.In: Nriagu JO, ed. *Arsenic in the Environment, Part II: Human Health and Ecosystem Effects*. New York: John Wiley & Sons, Inc., 17-34.

NORDLING CO, 1953. A New Theory on the Cancer-Inducing Mechanism. *British Journal of Cancer* 7:68-72.

ORMEROD MG, 1994. Futther Applications to Cell Biology.In: Ormerod MG, ed. *Flow Cytometry: A Practical Approach*. Oxford: Oirl Press, 261-273.

PETERS LJ, 1996. Radiation Therapy Tolerance Limits. For One or for All? - Janeway Lecture. *Cancer* 77:2379-2385.

PORTIER CJ, EDLER L, 1990. Two-Stage Models of Carcinogenesis, Classification of Agents, and Design of Experiments. *Fundamental and Applied Toxicology* 14:444-460.

POTT WA, BENJAMIN SA, YANG RSH, 1998. Antagonistic Interactions of an Arsenic-Containing Mixture in a Multiple Organ Carcinogenicity Bioassay. *Cancer Letters* 133:185-190.

PRASAD GL, FULDNER RA, COOPER HL, 1993. Expression of Transduced Tropomyosin 1 cDNA Suppresses Neoplastic Growth of Cells Transformed by the *ras* Oncogene. *Proceedings of the National Academy of Sciences of the United States of America* 90:7039-7043.

PRESTON GA, LANG JE, MARONPOT RR, BARRETT JC, 1994. Regulation of Apoptosis by Low Serum in Cells of Different Stages of Neoplastic Progression: Enhanced Susceptibility after Loss of a Senescence Gene and Decreased Susceptibility after Loss of a Tumor Suppressor Gene. *Cancer Research* 54:4214-4223.

PUTNAM RD, 1986. Review of Toxicity of Inorganic Lead. *American Industrial Hygiene Association Journal* 47:700-703.
Smith, T. B. Evaluation of Carcinogenic Potential of Chemical Mixtures Containing Arsenic and Volatile Organics. 1997. Colorado State University. Ref Type: Thesis/Dissertation

SPSS INC., 1997. *Transforms & Regressions Reference Manual for SigmaPlot*.Chicago: SPSS Inc., 8-23-8-31.

STEEL GG, 1977. Basic theory of growing cell populations.In: Steel GG, ed. *Growth kinetics of tumours: cell population kinetics in relation to the growth and treatment of cancer*. Oxford: Clarendon Press, 57-85.

TAN WY, 1991. Two-Stage Models of Carcinogenesis.In: *Stochastic Models of Carcinogenesis*. New York: Marcel Dekker, Inc., 81-133.

WEINBERG RA, 1996. How Cancer Arises. *Scientific American* 275:62-70.

WILSON GD, 1994. Analysis of DNA-Measurement of Cell Kinetics by the Bromodeoxyuridine/Anti-bromodeoxyuridine Method.In: Ormerod MG, ed. *Flow Cytometry: A Practical Approach*. Oxford: Oirl Press, 137-156.

YAMAUCHI H, FOWLER BA, 1994. Toxicity and Metabolism of Inorganic and Methylated Arsenicals.In: Nriagu JO, ed. *Arsenic in the Environment, Part II: Human Health and Ecosystem Effects*. New York: John Wiley & Sons, Inc., 35-53.

Appendix A: Calculations of potential doubling times

Part A. Data used to calculate the T_{pot} for normal cells in Figure 4.5*

Cell isolate	Passage	Sampling time (days after passage)	Relative movement (RM)	DNA synthesis time (Ts; hour)	Labeling index (LI)	Potential doubling time (T_{pot}; hour)
Control 36	p4	2 days	0.87	4.1	0.320	13
Control 40	p4	2 days	0.84	4.4	0.399	11
Control 43	p4	2 days	0.87	4.0	0.346	12
Control 15	p3	3 days	0.81	4.8	0.377	13
Control 39	p3	3 days	0.85	4.3	0.327	13
Control 43	p3	3 days	0.83	4.5	0.367	12
Control 38	p13	3 days	0.86	4.2	0.299	14
Control 36	p8	3 days	0.83	4.5	0.260	17
Control 38	p8	3 days	0.80	5.1	0.303	17
Control 40	p8	3 days	0.87	4.1	0.239	17
Control 38	p9	3 days	0.75	6.0	0.372	16
Control 36	p4	4 days	0.81	4.8	0.232	21
Control 40	p4	4 days	0.74	6.3	0.327	19
Control 15	p3	5 days	0.77	5.6	0.248	23
Control 36	p8	5 days	0.83	4.6	0.193	24
Control 38	p8	5 days	0.80	5.0	0.198	25
Control 40	p8	5 days	0.85	4.3	0.166	26
Control 29	p2	5 days	0.78	5.8	0.197	30
Control 38	p13	5 days	0.75	6.0	0.198	31
Control 27	p3	5 days	0.74	6.3	0.240	26
Control 34	p6	5 days	0.78	5.3	0.188	28
Control 19	p3	5 days	0.71	7.1	0.229	31
Control 15	p4	5 days	0.77	5.5	0.173	32

Part A. (Continued)

Cell isolate	Passage	Sampling time (days after passage)	Relative movement (RM)	DNA synthesis time (Ts; hour)	Labeling index (LI)	Potential doubling time (T_{pot}; hour)
Control 36	p9	6 days	0.74	6.2	0.112	55
Control 38	p9	6 days	0.73	6.5	0.102	63
Control 27	p4	6 days	0.71	7.1	0.109	65
Control 34	p7	6 days	0.70	7.5	0.161	46
Control 19	p4	6 days	0.66	9.2	0.142	65

* All sample were fixed by 70% ethanol at 3 hours after BrdU pulse-labeling

Part B. Data measured for growth inhibition study by arsenic*

Cell isolate	Passage	Sampling time (days after passage)	Relative movement (RM)	DNA synthesis time (Ts; hour)	Labeling index (LI)	Potential doubling time (T_{pot}; hour)
Control I	p4	3 days	0.81	4.8	0.395	12
Arsenic 0.5	p4	3 days	0.82	4.7	0.342	14
Arsenic 1.0	p4	3 days	0.79	5.2	0.362	14
Arsenic 2.0	p4	3 days	0.81	4.8	0.315	15
Arsenic 5.4	p3	3 days	0.78	5.3	0.128	42
Arsenic 5.4	p4	3 days	0.77	5.6	0.114	50
Control I	p4	5 days	0.75	6.0	0.243	25
Arsenic 0.5	p4	5 days	0.79	5.2	0.237	22
Arsenic 1.0	p4	5 days	0.76	5.7	0.221	26
Arsenic 2.0	p4	5 days	0.75	6.0	0.235	25
Arsenic 5.4	p3	5 days	0.74	6.3	0.086	74
Arsenic 5.4	p4	5 days	0.76	5.8	0.062	94

* All sample were fixed by 70% ethanol at 3 hours after BrdU pulse-labeling

Appendix B: Optimization of cell death rate

```
%This is a program written in Matlab to optimize cell death rates by
%"fmins" command, a built-in function in Matlab to minimize the given
%function using a Nelder-Mead type simplex search method, with function
%file "Dr_mf". Function file "Dr_df" is used to solve differential
%equations.

clear

tc=[0 24 50.25];                %Sampling times (h)
Nc=[9.25E4 2.00E5 5.125E5];     %Experimental data of live cells
Dc=[1073 2060 3792.5];          %Experimental data of dead cells

r=2;  %Heteroscedasticity parameter in Objective Function; r=2: relative
      %weighting
BN=fmins('Dr_mf',[0.00027 Nc(1) Dc(1)],[],[],r,tc,Nc,Dc);
      %BN: optimization results; In parenthesis after fmins: filename of
      %function file, initial guess, options, blank, and parameters
      %passed to function file;
beta=BN(1)  %Cell death rate (h^-1)
N0=BN(2:3)  %Optimized initial numbers of live and dead cells

[t,N]=ode23('Dr_df',[0:1:60],N0,[],beta);
      %ode23: the built-in function in Matlab for solving ordinary
      %differential equation using Runge-Kutta 2nd order algorithm; N:
      %the solutions for differential equations with respect to time, t
      %(h); N(1):live cells, N(2): dead cells. In parenthesis after
      %ode23: filename of function file, time span, initial values,
      %blank, parameter passed to function file.

semilogy(t,N,tc,Nc,'o',tc,Dc,'^')   %Plot experimental and simulation
                                    %data on semi-log plot
xlabel('Time (h)')
ylabel('Cell Number')
title('Prediction of Death Rate')


--------------------------------------------------------------------------
%This is the function file, "Dr_mf", to optimize cell death rate

function err=Dr_mf(BN,r,tc,Nc,Dc)
      %err: function to be minimized; BN: variables to be adjusted; r,
      %tc, Nc, Dc: parameters passed from main program

beta=BN(1); %Cell death rate (h^-1)
```

```
N0=BN(2:3); %Optimized initial numbers of live and dead cells

[t,N]=ode23('Dr_df',[tc 60],N0,[],beta);  %Solving differential
                                          %equations
err=0;
for i=1:length(Dc)
   err1=(N(i,1)-Nc(I)).^2./Nc(I).^r;      %Objective function for live
                                          %cells
   err2=(N(i,2)-Dc(I)).^2./Dc(I).^r;      %Objective function for dead
                                          %cells
   err=err+err1+err2;
end

-------------------------------------------------------------------------
%This is the function file, "Dr_df", to solve differential equations

function NP=Dr_df(t,N,init,beta)
      %NP(1): dN/dt; NP(2): dD/dt; init: default setting; beta: cell
      %death rate passed from main program.
p1=4.1309e-63; p2=-4.4119e-56;
p3=2.0404e-49; p4=-5.3603e-43;
p5=8.8249e-37; p6=-9.4923e-31;
p7=6.7745e-25; p8=-3.2320e-019;
p9=1.0824e-013; p10=-5.3390e-8; p11=0.0554;

alfa=p1*N(1).^10+p2*N(1).^9+p3*N(1).^8+p4*N(1).^7+p5*N(1).^6+p6*N(1).^5+
p7*N(1).^4+p8*N(1).^3+p9*N(1).^2+p10*N(1).^1+p11;
      %alfa: cell division rates (h^-1), functions of cell number per
      %dish, N(1), fitted by a polynomial of degree 10.

NP(1,:)=N(1).*(alfa-beta);     %dN/dt=N*(alfa-beta)
NP(2,:)=N(1).*beta;            %dD/dt=N*beta
```

Appendix C: Optimization of lag time

```
%This is a program written in Matlab to optimize lag time by "fmins"
%command, a built-in function in Matlab to minimize the given function
%using a Nelder-Mead type simplex search method, with function file
%"Tl_mf".  Function file "Tl_df" is used to solve differential
%equations.

clear
N0=4e4;      %Initial number of normal cell per dish

tc7=[69.5 93.25 117.5];              %Experimental data of sampling time
Nc38_7=[2.35E5 3.75E5 9.70E5];       %Experimental data of cell number
tc8=[71.33 95.17 112.5];             %Experimental data of sampling time
Nc38_8=[2.70E5 4.90E5 8.50E5];       %Experimental data of cell number

[tc I]=sort([tc7 tc8]); %Data collected from different experiments are
                        %sorted by magnitude for optimization program
Nns=[Nc38_7 Nc38_8];
Nc=Nns(I);

r=2;  %Heteroscedasticity parameter; r=2: relative weighting
Tlag=fmins('Tl_mf',[42.4],[],[],r,tc,Nc)
      %Tlag: optimization result of lag time; In parenthesis after
      %fmins: filename of function file, initial guess, options, blank,
      %and parameters passed to function file;

[t,N]=ode23('Tl_df',[Tlag 43:1:168],N0);
      %ode23: the built-in function in Matlab for solving ordinary
      %differential equation using Runge-Kutta 2nd order algorithm; N:
      %number of normal cells solved by differential equations with
      %respect to time, t (h). In parenthesis after ode23: filename of
      %function file, time span, initial values.

y0=12.4363; a=9.132E2; b=4.323E2;
Tpot=y0+a*exp(b*t);      %Potential doubling time (h); a function of
                         %time, t

plot([0;t],[N0;N],tc7,Nc38_7,'x',tc8,Nc38_8,'o')
      %Plot predicted and experimental results
xlabel('Time after cells being passaged (h)')
ylabel('Cell Number')
title('Simulation of the Growth of NORMAL Cell within One Passage')
```

```
%This is the function file, "Tl_mf", to optimize lag time

function err=Tl_mf(Tlag,r,tc,Nc)
      %err: function to be minimized; Tlag: variables to be adjusted;
      %r, tc, Nc: parameters passed from main program.

N0=4e4;     %Initial number of normal cell per dish
[t,N]=ode23('Tl_df',[Tlag tc 168],N0);
      %Solving differential equations

err=0;
for i=1:length(tc)
   err1=(N(I+1)-Nc(I)).^2./Nc(I).^r;      %Objective function for normal
                                          %cells
   err=err+err1;
end
```

```
%This is the function file, "Tl_df", to solve differential equations

function NP=Tl_df(t,N)        %NP: dN/dt

y0=12.4363; a=9.132E-2; b=4.323E-2;
Tpot=y0+a*exp(b*t);     %Potential doubling time; a function of time, t

alfa(1)=log(2)/Tpot;    %Cell division rate (h^-1); alfa=(ln 2)/Tpot
beta(1)=0.000295;       %Cell death rate (h^-1)

NP(1,:)=N(1).*(alfa(1)-beta(1));    %dN/dt=N*(alfa-beta)
```

Appendix D: BBDR model of the growth of SHE cells

```
%This is a program written in Matlab to model the growth of SHE cells.

clear
N0p1=4e4.*ones(3,1);     %Initial number of normal cells at passage 1

%For Passage 1
[ttp1,N2p1(:,1)]=ode23('mdl_tf1',[41.9,43:1:168],N0p1(1));
      %ode23: the built-in function in Matlab for solving ordinary
      %differential equation using Runge-Kutta 2nd order algorithm;
      %N2p1(:,1) number of normal cells in exponential growth phase
      %solved by differential equations with respect to time, ttp1. In
      %parenthesis after ode23: filename of function file, time span,
      %initial value.
tp1=[0;ttp1];      %Time points in Passage 1; exponential and lag phases
Np1(:,1)=[N0p1(1);N2p1(:,1)];        %Normal cell number in Passage 1;
                                     %exponential and lag phases
N0p2(1)=N2p1(length(N2p1(:,1)),1);  %Initial number for Passage 2

   %For upper bound of uncertainty of model in Passage 1
   [ttp1,N2p1(:,2)]=ode23('mdl_tfe',[41.9,43:1:168],N0p1(2),[],1);
      %N2p1(:,2) upper bound of normal cells in exponential growth phase
      %solved by differential equations with respect to time, ttp1. In
      %parenthesis after ode23: filename of function file, time span,
      %initial value, blank, parameter passed to function file (1: upper
      %bound).
   N0p2(2)=N2p1(length(N2p1(:,2)),2);
      %Upper bound of normal cell number in Passage 1; exponential and
      %lag phases
   Np1(:,2)=[N0p1(2);N2p1(:,2)];
      %Initial value for upper bound in Passage 2

   %For lower bound of uncertainty of model in Passage 1
   [ttp1,N2p1(:,3)]=ode23('mdl_tfe',[41.9,43:1:168],N0p1(3),[],-1);
      %N2p1(:,3) lower bound of normal cells in exponential growth phase
      %solved by differential equations with respect to time, ttp1. In
      %parenthesis after ode23: filename of function file, time span,
      %initial value, blank, parameter passed to function file (-1:
      %lower bound).
   N0p2(3)=N2p1(length(N2p1(:,3)),3);
      %Lower bound of normal cell number in Passage 1; exponential and
      %lag phases
   Np1(:,3)=[N0p1(3);N2p1(:,3)];
      %Initial value for lower bound in Passage 2
```

```
%For Passage 2; refer to the section of Passage 1
[ttp2,N2p2(:,1)]=ode23('mdl_tf1',[41.9,43:1:168],N0p2(1));
tp2=[tp1(length(tp1));ttp2+tp1(length(tp1))];
      %Transfer the time points from those based on single passage
      %(ttp2) to based on life span (tp2); the differential equation was
      %solved at time points based on single passage since the potential
      %doubling times are functions of time after passage
Np2(:,1)=[N0p2(1);N2p2(:,1)];
N0p3(1)=N2p2(length(N2p2(:,1)),1);
   %For upper bound of uncertainty of model in Passage 2
   [ttp2,N2p2(:,2)]=ode23('mdl_tfe',[41.9,43:1:168],N0p2(2),[],1);
   N0p3(2)=N2p2(length(N2p2(:,2)),2);
   Np2(:,2)=[N0p2(2);N2p2(:,2)];
   %For lower bound of uncertainty of model in Passage 2
   [ttp2,N2p2(:,3)]=ode23('mdl_tfe',[41.9,43:1:168],N0p2(3),[],-1);
   N0p3(3)=N2p2(length(N2p2(:,3)),3);
   Np2(:,3)=[N0p2(3);N2p2(:,3)];

%For Passage 3; refer to the section of Passage 1 and 2
[ttp3,N2p3(:,1)]=ode23('mdl_tf1',[41.9,43:1:192],N0p3(1));
tp3=[tp2(length(tp2));ttp3+tp2(length(tp2))];
Np3(:,1)=[N0p3(1);N2p3(:,1)];
N0p4(1)=N2p3(length(N2p3(:,1)),1);
   %For upper bound of uncertainty of model in Passage 3
   [ttp3,N2p3(:,2)]=ode23('mdl_tfe',[41.9,43:1:192],N0p3(2),[],1);
   N0p4(2)=N2p3(length(N2p3(:,2)),2);
   Np3(:,2)=[N0p3(2);N2p3(:,2)];
   %For lower bound of uncertainty of model in Passage 3
   [ttp3,N2p3(:,3)]=ode23('mdl_tfe',[41.9,43:1:192],N0p3(3),[],-1);
   N0p4(3)=N2p3(length(N2p3(:,3)),3);
   Np3(:,3)=[N0p3(3);N2p3(:,3)];

%For Passage 4; refer to the section of Passage 1 and 2
[ttp4,N2p4(:,1)]=ode23('mdl_tf1',[41.9,43:1:216],N0p4(1));
tp4=[tp3(length(tp3));ttp4+tp3(length(tp3))];
Np4(:,1)=[N0p4(1);N2p4(:,1)];
N0p5(1)=N2p4(length(N2p4(:,1)),1);
   %For upper bound of uncertainty of model in Passage 4
   [ttp4,N2p4(:,2)]=ode23('mdl_tfe',[41.9,43:1:216],N0p4(2),[],1);
   N0p5(2)=N2p4(length(N2p4(:,2)),2);
   Np4(:,2)=[N0p4(2);N2p4(:,2)];
   %For lower bound of uncertainty of model in Passage 4
   [ttp4,N2p4(:,3)]=ode23('mdl_tfe',[41.9,43:1:216],N0p4(3),[],-1);
   N0p5(3)=N2p4(length(N2p4(:,3)),3);
   Np4(:,3)=[N0p4(3);N2p4(:,3)];

%For Passage 5; refer to the section of Passage 1 and 2
[ttp5,N2p5(:,1)]=ode23('mdl_tf1',[41.9,43:1:168],N0p5(1));
tp5=[tp4(length(tp4));ttp5+tp4(length(tp4))];
Np5(:,1)=[N0p5(1);N2p5(:,1)];
N0p6(1)=N2p5(length(N2p5(:,1)),1);
   %For upper bound of uncertainty of model in Passage 5
   [ttp5,N2p5(:,2)]=ode23('mdl_tfe',[41.9,43:1:168],N0p5(2),[],1);
   N0p6(2)=N2p5(length(N2p5(:,2)),2);
```

```
   Np5(:,2)=[N0p5(2);N2p5(:,2)];
   %For lower bound of uncertainty of model in Passage 5
   [ttp5,N2p5(:,3)]=ode23('mdl_tfe',[41.9,43:1:168],N0p5(3),[],-1);
   N0p6(3)=N2p5(length(N2p5(:,3)),3);
   Np5(:,3)=[N0p5(3);N2p5(:,3)];


tcount=[0,168,336,528,744];    %Sampling times for groups other than 5.4
                               %μM of As
tcount54=[0,168,336,528,768]; %Sampling times for cells exposed to 5.4
                               %μM of As
N_ctrl=[4.00E4 3.06E6 1.90E8 1.25E10 8.39E11];
      %Cell counts for control cells
N_as05=[4.00E4 2.08E6 9.98E7 5.39E9 2.10E11];
      %Cell counts for cells exposed to 0.5 μM of As
N_as1=[4.00E4 1.88E6 9.40E7 4.89E9 1.71E11];
      %Cell counts for cells exposed to 1 μM of As
N_as2=[4.00E4 1.48E6 4.74E7 1.99E9 7.76E10];
      %Cell counts for cells exposed to 2 μM of As
N_as54=[4.00E4 1.20E6 2.64E7 1.32E8 4.62E8];
      %Cell counts for cells exposed to 5.4 μM of As

%Plot predicted and experimental results
semilogy(tp1,Np1(:,1),tp2,Np2(:,1),tp3,Np3(:,1),tp4,Np4(:,1),tp5,Np5(:,1
))
hold on
semilogy(tp1,Np1(:,2:3),'-.',tp2,Np2(:,2:3),'-.',tp3,Np3(:,2:3),'-
.',tp4,Np4(:,2:3),'-.',tp5,Np5(:,2:3),'-.')
semilogy(tcount,N_ctrl,'+',tcount,N_as05,'p',tcount,N_as1,'s',tcount,N_a
s2,'d',tcount54,N_as54,'h')
hold off

xlabel('Time after passage (h)')
ylabel('Cell Number')
title('Simulation of Cell Growth through 5 Passages')


-------------------------------------------------------------------------
%This is the function file, "mdl_tf1", to solve differential equation

function NP=mdl_tf1(t,N)       %NP: dN/dt

y0=12.4363; a=9.132E-2; b=4.323E-2;
Tpot=y0+a*exp(b*t);      %Potential doubling time; function of time, t
alfa(1)=log(2)/Tpot;     %Cell division rate; alfa=(ln 2)/Tpot
beta(1)=0.000295;        %Cell death rate

NP(1,:)=N(1).*(alfa(1)-beta(1));     %dN/dt=N*(alfa-beta)


-------------------------------------------------------------------------
%This is the function file, "mdl_tfe", to solve differential equations

function NP=mdl_tfe(t,N,init,P1)
```

```
      %NP: dN/dt; init: default setting; P1: parameter passed from main
      %program.


y0=12.4363;
a=9.132E-02;
b=4.323E-02;

if P1==0     %Cell division rate calculated by the mean of Tpot
   Tpot=y0+a*exp(b*t);  %Potential doubling time; function of time, t
elseif P1>0 %Upper bound; cell division rate calculated by Tpot +
            %standard error of estimating Tpot
   Tpot=1.7454+y0+a*exp(b*t);
else        %Lower bound; cell division rate calculated by Tpot -
            %standard error of estimating Tpot
   Tpot=-1.7454+y0+a*exp(b*t);
end

alfa(1)=log(2)/Tpot;     %Cell division rate; alfa=(ln 2)/Tpot
beta(1)=0.000295;        %Cell death rate

NP(1,:)=N(1).*(alfa(1)-beta(1));     %dN/dt=N*(alfa-beta)
```

Appendix E: Optimization of potential doubling time

```
%This is a program written in Matlab to optimize lag time by "fmins"
%command, a built-in function in Matlab to minimize the given function,
%i.e. optimize the factor that the mean of potential doubling time have
%to be multiplied by to provide best prediction of control cell line,
%using a Nelder-Mead type simplex search method, with function file
%"Tl_mf". Function file "Tl_df" is used to solve differential
%equations.

clear
N0=4e4;     %Initial number of normal cell per dish

r=2;        %Heteroscedasticity parameter; r=2: relative weighting
Sigma=fmins('Si_mf',[1],[],[],r)
      %Sigma: optimization result of the factor that the mean of
      %potential doubling time have to be multiplied by to provide best
      %prediction of control cell line; In parenthesis after fmins:
      %filename of function file, initial guess, options, blank, and
      %parameters passed to function file;

[t,N]=ode23('Si_df',[41.9 43:1:168],N0,[],Sigma);
      %ode23: the built-in function in Matlab for solving ordinary
      %differential equation using Runge-Kutta 2nd order algorithm; N:
      %number of normal cells solved by differential equations with
      %respect to time, t. In parenthesis after ode23: filename of
      %function file, time span, initial values, blank, parameter passed
      %to function file.

y0=12.4363; a=9.132E-02; b=4.323E-02;
Tpot=y0+a*exp(b*t);     %Potential doubling time; function of time, t

%The next section is the simulation of cell growth through 5 passages

%Passage 1
N0p(1)=4e4;       %Initial number of normal cells at passage 1
[ttp1,N2p1]=ode23('Si_df',[41.9 43:1:168],N0p(1),[],Sigma);
      %N2p1 number of normal cells in exponential growth phase solved by
      %differential equations with respect to time, ttp1. In parenthesis
      %after ode23: filename of function file, time span, initial value,
      %parameter (optimized result) passed to function file.
tp1=[0;ttp1];     %Time points in Passage 1; exponential and lag phases
Np1=[N0p(1);N2p1];      %Normal cell number in Passage 1; exponential
                        %and lag phases
N0p(2)=N2p1(length(N2p1));    %Initial number for Passage 2
```

```
%Passage 2
[ttp2,N2p2]=ode23('Si_df',[41.9 43:1:168],N0p(2),[],Sigma);
tp2=[tp1(length(tp1));ttp2+tp1(length(tp1))];

      %Transfer the time points from those based on single passage
      %(ttp2) to based on life span (tp2); the differential equation was
      %solved at time points based on single passage since the potential
      %doubling times are functions of time after passage.
Np2=[N0p(2);N2p2];
N0p(3)=N2p2(length(N2p2));

%Passage 3
[ttp3,N2p3]=ode23('Si_df',[41.9 43:1:192],N0p(3),[],Sigma);
tp3=[tp2(length(tp2));ttp3+tp2(length(tp2))];
Np3=[N0p(3);N2p3];
N0p(4)=N2p3(length(N2p3));

%Passage 4
[ttp4,N2p4]=ode23('Si_df',[41.9 43:1:216],N0p(4),[],Sigma);
tp4=[tp3(length(tp3));ttp4+tp3(length(tp3))];
Np4=[N0p(4);N2p4];
N0p(5)=N2p4(length(N2p4));

%Passage 5
[ttp5,N2p5]=ode23('Si_df',[41.9 43:1:168],N0p(5),[],Sigma);
tp5=[tp4(length(tp4));ttp5+tp4(length(tp4))];
Np5=[N0p(5);N2p5];

tcount=[0,168,336,528,744];   %Sampling times for groups other than 5.4
                              %μM of As
tcount54=[0,168,336,528,768]; %Sampling times for cells exposed to 5.4
                              %μM of As
N_ctrl=[4.00E4 3.06E6 1.90E8 1.25E10 8.39E11];
      %Cell counts for control cells
N_as05=[4.00E4 2.08E6 9.98E7 5.39E9 2.10E11];
      %Cell counts for cells exposed to 0.5 μM of As
N_as1=[4.00E4 1.88E6 9.40E7 4.89E9 1.71E11];
      %Cell counts for cells exposed to 1 μM of As
N_as2=[4.00E4 1.48E6 4.74E7 1.99E9 7.76E10];
      %Cell counts for cells exposed to 2 μM of As
N_as54=[4.00E4 1.20E6 2.64E7 1.32E8 4.62E8];
      %Cell counts for cells exposed to 5.4 μM of As

%Plot predicted and experimental results
figure
semilogy(tp1,Np1,tp2,Np2,tp3,Np3,tp4,Np4,tp5,Np5)
hold on
semilogy(tcount,N_ctrl,'+',tcount,N_as05,'p',tcount,N_as1,'s',tcount,N_a
s2,'d',tcount54,N_as54,'h')
hold off
xlabel('Time after passage (h)')
ylabel('Cell Number')
title('Simulation of Cell Growth through 5 Passages')
```

```
%The next section is the curve fitting of cell division rate versus cell
%number per dish
p=polyfit(N,log(2)./(Sigma.*Tpot),10);
      %Finds the coefficients of a polynomial P(N) of degree 10 that
      %fits the data in a least-squares sense; log(2)./(Sigma*Tpot):
      %cell division rate.

%Plot the curve fitting and experimental results
figure
plot(N,log(2)./(Sigma.*Tpot))
hold on
plot(N,polyval(p,N),'+')
hold off
xlabel('Cell number per plate')
ylabel('Division rate, alfa (1/h)')
title('Cell division rate versus cell density')


--------------------------------------------------------------------------
%This is the function file, "Si_mf", to optimize the factor that the
%mean of potential doubling time have to be multiplied by to provide
%best prediction of control cell line.

function err=Si_mf(Sigma,r)
      %err: function to be minimized; Sigma: variables to be adjusted;
      %r: parameter passed from main program.

%The next section is the simulation of cell growth through 5 passages;
%refer to main program illustrated above

N0p(1)=4e4;
[ttp1,N2p1]=ode23('Si_df',[41.9 43:1:168],N0p(1),[],Sigma);    %120
tp1=[0;ttp1];
Np1=[N0p(1);N2p1];
N0p(2)=N2p1(length(N2p1));

[ttp2,N2p2]=ode23('Si_df',[41.9 43:1:168],N0p(2),[],Sigma);    %216
tp2=[tp1(length(tp1));ttp2+tp1(length(tp1))];
Np2=[N0p(2);N2p2];
N0p(3)=N2p2(length(N2p2));

[ttp3,N2p3]=ode23('Si_df',[41.9 43:1:192],N0p(3),[],Sigma);    %192
tp3=[tp2(length(tp2));ttp3+tp2(length(tp2))];
Np3=[N0p(3);N2p3];
N0p(4)=N2p3(length(N2p3));

[ttp4,N2p4]=ode23('Si_df',[41.9 43:1:216],N0p(4),[],Sigma);    %216
tp4=[tp3(length(tp3));ttp4+tp3(length(tp3))];
Np4=[N0p(4);N2p4];
N0p(5)=N2p4(length(N2p4));

[ttp5,N2p5]=ode23('Si_df',[41.9 43:1:168],N0p(5),[],Sigma);
tp5=[tp4(length(tp4));ttp5+tp4(length(tp4))];
Np5=[N0p(5);N2p5];
```

```
tcount=[0,168,336,528,744];
N_ctrl=[4.00E+04 3.06E+06 1.90E+08 1.25E+10 8.39E+11];

err=0;
for i=2:length(N_ctrl)
   err1=(N0p(i)-N_ctrl(i)).^2./N_ctrl(i).^r;     %Objective function
   err=err+err1;
end
```

```
%This is the function file, "Si_df", to solve differential equations

function NP=Si_df(t,N,init,Sigma)
      %NP: dN/dt; init: default setting; Sigma: parameter passed from
      %main program.

y0=12.4363; a=9.132E-02; b=4.323E-02;
Tpot=y0+a*exp(b*t);      %Potential doubling time; function of time, t

alfa(1)=log(2)/(Sigma*Tpot);  %Cell division rate; alfa=(ln2)/Sigma*Tpot
beta(1)=0.000295;             %Cell death rate

NP(1,:)=N(1).*(alfa(1)-beta(1));     %dN/dt=N*(alfa-beta)
```

Appendix F: Prediction of the growth of a mixed cell population

```
%This is a program written in Matlab to predict the growth of a mixed
%cell population including normal and senescent cells, where the cell
%division rates are optimized using 2 experimental data for Tpot and 1
%data from cell counts. A 3-parameter exponential equation is used to
%predict the distribution of Tpot via the "fmins" command, a built-in
%function in Matlab to minimize the given function using a Nelder-Mead
%type simplex search method, with function files "Cf_mf" and "Cf_cff".
%Function file "Cf_df" is used to solve differential equations.

clear

tf=192; Nf=2e5;    %Nf is cell number counted at time tf
Tpm=[42 74];       %TpotS measured at 72 and 120 hours after passage

N0=4e4;      %Initial cell number

Tpf=fmins('Cf_mf',[1000],[],[],Tpm,tf,Nf)
      %Tpf: optimized result for the Tpot at time tf; In parenthesis
      %after fmins: filename of function file, initial guess, options,
      %blank, and parameters passed to function file;

ts=[72 120 tf]';  %Sampling times, 72, 120, and tf hours after passage
Tp=[Tpm Tpf]';    %TpotS; experimental data Tpm and optimized result Tpf

%The distribution of Tpot is optimized using function file "Cf_mf" as
%described above. The next 4 lines are used to calculate the optimized
%result via the equation Tpot=c(1)+c(2)*exp(lambda*t) which is written in
%a matrix form Tp=A*c; Tp denotes Tpot; t is time after passage. Details
%are described in the function file "Cf_mf".
lambda=fmins('Cf_cff',0.01,[],[],ts,Tp);
A(:,1)=ones(length(ts),1);
A(:,2)=exp(lambda.*ts);
c=A\Tp;

[t,N]=ode23('Cf_df',[41.9,43:1:tf],N0,[],lambda,c);
      %ode23: the built-in function in Matlab for solving ordinary
      %differential equation using Runge-Kutta 2nd order algorithm; N:
      %total cell numbers solved by differential equations with respect
      %to time t. In parenthesis after ode23: filename of function file,
      %time span, initial value, blank, parameters passed to function
      %file ("lambda" and "c" allow function file to use optimized Tpot
      %distribution to calculate cell division rate).
```

```
%Plot experimental and predicted results
plot(t,N,tf,Nf,'^')
xlabel('Time after passage (h)')
ylabel('Cell Number')
title('Cell Number vs. Time for As 5.4 p3')
```

```
%This is the function file, "Cf_mf", to optimize the distribution of Tpot
%using 2 experimental data for Tpot and 1 data from cell counts via the
%equation Tpot=c(1)+c(2)*exp(lambda*t); t: time after passage

function err=Cf_mf(Tpf,Tpm,tf,Nf)
      %err: function to be minimized; Tpf: variables to be adjusted;
      %Tpm, tf, Nf: parameter passed from main program.

N0=4e4;      %Initial cell number
ts=[72 120 tf]';  %Sampling times, 72, 120, and tf hours after passage
Tp=[Tpm Tpf]';    %TpotS; experimental data (Tpm) and value to be
                  %optimized Tpf

%The next section is to optimize the 3 parameters (c(1), c(2), lambda)
%in the equation Tpot=c(1)+c(2)*exp(lambda*t) which is written in matrix
%form Tp=A*c; Tp denotes Tpot
lambda=fmins('Cf_cff',0.01,[],[],ts,Tp);
      %lambda: optimized result; In parenthesis after fmins: filename of
      %function file, initial guess, options, blank, and parameters
      %passed to function file;
A(:,1)=ones(length(ts),1);
A(:,2)=exp(lambda.*ts);
c=A\Tp;

[t,N]=ode23('Cf_df',[41.9,43:1:tf],N0,[],lambda,c);
      %Solve differential equation; N: total cell numbers solved by
      %differential equations with respect to time t. In parenthesis
      %after ode23: filename of function file, time span, initial value,
      %blank, parameters passed to function file ("lambda" and "c" allow
      %function file to use optimized Tpot distribution to calculate cell
      %division rate).

err=abs(N(length(N))-Nf)      %Error of the predicted cell number at
                              %time tf
```

```
%This is the function file, "Cf_cff", to optimize the 3 parameters
%(c(1), c(2), lambda) in the equation Tpot=c(1)+c(2)*exp(lambda*t) which
%is written in matrix form Tp=A*c; Tp denotes Tpot

function err = Cf_cff(lambda,ts,Tp)
      %err: function to be minimized; lambda: variables to be adjusted;
      %ts, Tp: parameter passed from main program.
A(:,1)=ones(length(ts),1);
A(:,2)=exp(lambda.*ts);
```

```
c = A\Tp;
z = A*c;            %Predicted values for Tpots

err = norm(z-Tp); %Norm of the vector containing errors between
                  %predicted values (z) and experimental data (Tp)


--------------------------------------------------------------------------
%This is the function file, "Cf_df", to solve differential equations

function NP=Cf_df(t,N,init,lambda,c)
      %NP: dN/dt; init: default setting; lambda, c: parameters passed
      %from main program.

%Cell division rates are calculated by the optimized Tpot distribution:
%Tpot=c(1)+c(2)*exp(lambda*t) which is written in matrix form Tp=A*c; Tp
%denotes Tpot
A(:,1)=ones(length(t),1);
A(:,2)=exp(lambda.*t);
Tpot=A*c;

alfa(1)=log(2)./Tpot;    %Cell division rate; alfa=(ln2)/Tpot
beta(1)=0.000295;        %Cell death rate

NP(1,:)=N(1).*(alfa(1)-beta(1));     %dN/dt=N*(alfa-beta)
```

Appendix G: Optimization of senescence rate without adjusting division rates

```
!This is a program written in ACSL to optimize cell senescence rates γ
!by ACSL Optimize with the parameter saved in "Cr3.m" file.

PROGRAM      Senescence rate estimation

INITIAL

  VARIABLE TIME=0.
  CONSTANT N0=4e4          !Initial number of normal cells
  CONSTANT S0=0.0          !Initial number of senescent cells
  CONSTANT gamma1=0.0574       !Initial guess for γ at 3rd passage
  CONSTANT gamma2=0.0574       !Initial guess for γ at 4th passage
  CONSTANT beta=0.000295       !Cell death rate (1/h)
  !Constants start with "p" are the parameters in the polynomial which
  !describes the relation between cell division rates and cell numbers
  CONSTANT p1=4.1462e-64, p2=-5.9308e-57, p3=3.6672e-50
  CONSTANT p4=-1.2847e-43, p5=2.8100e-37, p6=-3.9935e-31
  CONSTANT p7=3.7338e-25, p8=-2.3013e-19, p9=9.6871e-14
  CONSTANT p10=-5.0492e-8, p11=0.05912858
  TSTOP=432.       !Length of experiments (hour)
  POINTS=TSTOP*2.  !Number of points in plot
  CINT=TSTOP/POINTS      !Communication interval

END    !End of Initial Segment

DYNAMIC

  DERIVATIVE
      !Lag phase at passage 3
      IF (TIME .LE. 41.9) THEN
      RN=0.         !RN: Rate of change for normal cell #
      RS=0.         !RS: Rate of change for senescent cell #

      !Exponential growth phase at passage 3
      ELSE IF (TIME .LE. 192.) THEN
      alfa=p1*NS**10+p2*NS**9+p3*NS**8+p4*NS**7+p5*NS**6+p6*NS**5+&
      p7*NS**4+p8*NS**3+p9*NS**2+p10*NS**1+p11
      !alfa: cell division rate (1/h); function of cell number; NS:
      !total # of cells
      RN=N*(alfa-beta-gamma1)        !N: normal cell #
      RS=N*gamma1


      !Lag phase at passage 4
```

```
      ELSE IF (TIME .LE. 233.9) THEN
      RN=0.
      RS=0.
      NS30=NS

      !Exponential growth phase at passage 4
      ELSE
      NSF=NS*4e4/NS30
      !Convert accumulated total cell # (NS) to total cell # in single
      !dish (NSF)
      alfa=p1*NSF**10+p2*NSF**9+p3*NSF**8+p4*NSF**7+p5*NSF**6+p6*NSF**5&
      +p7*NSF**4+p8*NSF**3+p9*NSF**2+p10*NSF**1+p11
      RN=N*(alfa-beta-gamma2)
      RS=N*gamma2
      END IF

      N=INTEG(RN,N0)     !Integrate RN (dN/dt) with initial value N0
      S=INTEG(RS,S0)     !Integrate RS (dS/dt) with initial value S0
      NS=N+S

  END !End of Derivative Segment

 TERMT(TIME .GE. TSTOP)

END   !End of Dynamic Segment

END   !End of program
```

```
!This is the command file

! File: CR3.cmd
set weditg=.false.       !suppress output from schedule
set hvdprn=.false.       !suppress hihg volume display
output /clear            !suppress output
PREPARE TIME,N,S,NS
start              !run the simulation as soon as loaded
```

```
%This is the m file which saved the parameters of optimization

% File: Cr3.m

% Optimization algorithm
% Values: 0 test run, 1 default, 2 Nelder-Mead, 3 GRG2
OpAlgorithm = 3

% Do not use the data set feature.
OpDataSets = []
% Experimental data
% The data values themselves.
OpExperData = [ ...
gamma]
```

```
% The names of the data matrices.
% (Used for display only.)
OpDataNames = [ ...
"gamma" ]
% The enable/disable flags for data matrices.
% (Used for display only.)
OpEnable = [ ...
1 ]'

% Model variables to fit against experimental data.
OpTargetNames = [ ...
"NS" ...
"S" ]
% Error model.  Rows correspond to variables being fit.
% First column: heteroscedasticity parameter.
% Second column: whether to vary heteroscedasticity parameter or hold it
fixed.
OpErrModel= [ ...
2 0
2 0]

% ACSL constants to be adjusted as parameters.
OpAdjustable= [ ...
"GAMMA1"
"GAMMA2" ]'
% Starting values.
OpStartValues = [ ...
        0.0574
        0.0574 ]'
% Constrained parameters (if any).
OpConstrained= [ ...
"GAMMA1"
"GAMMA1"
"GAMMA2"
"GAMMA2" ]'
% Constraints (if any).
OpConstraints = [ ...
             0             -1
             1              1
         0.057             -1
             1              1 ]

OpDescriptors = [ ]
OpExogColumns = [ ]
% Descriptor values
% Descriptor values for the enabled data matrices
OpAllExpers = []
OpExperiments = []
% Exogenous data
OpAllExogNames = []
% No exogenous data are present.
OpExogData = []

% Scripts run for each experiment.
```

```
% No special commands are run before each experiment is simulated.
OpScriptNames = []
OpAllScriptNames = []

% Whether objective function is displayed during parameter estimation.
OpVerbose=0

% Whether we run scripts at conclusion
% 0 = run no scripts, 1 = run if successful, 2 = run always
OpConcludeAct=1

% Script or scripts if any to run at conclusion.
OpConcludeScript=[ ...
"cmpplain"
"setop" ]

% End of file
```

Appendix H: Optimization of senescence rate with corrected division rates

```
!This is a program written in ACSL to optimize cell senescence rates γ
!with modified division rate (multiplied division rate α by a factor δ)
!using ACSL Optimize with the parameter saved in "Cr5.m" file.

PROGRAM      Senescence rate estimation with modified division rate

INITIAL

  VARIABLE TIME=0.
  CONSTANT N0=4e4          !Initial number of normal cells
  CONSTANT S0=0.0          !Initial number of senescent cells
  CONSTANT gamma1=0.0574       !Initial guess for γ at 3rd passage
  CONSTANT gamma2=0.0574       !Initial guess for γ at 4th passage
  CONSTANT beta=0.000295       !Cell death rate (1/h)
  CONSTANT delta=1.            !Initial guess for δ
  !Constants start with "p" are the parameters in the polynomial which
  !describes the relation between cell division rates and cell numbers
  CONSTANT p1=4.1462e-64, p2=-5.9308e-57, p3=3.6672e-50
  CONSTANT p4=-1.2847e-43, p5=2.8100e-37, p6=-3.9935e-31
  CONSTANT p7=3.7338e-25, p8=-2.3013e-19, p9=9.6871e-14
  CONSTAnT p10=-5.0492e-8, p11=0.05912858
  TSTOP=432.               !Length of experiments (hour)
  POINTS=TSTOP*2.          !Number of points in plot
  CINT=TSTOP/POINTS        !Communication interval

END   !End of Initial Segment

DYNAMIC

  DERIVATIVE

      !Lag phase at passage 3
      IF (TIME .LE. 41.9) THEN
      RN=0.        !RN: Rate of change for normal cell #
      RS=0.        !RS: Rate of change for senescent cell #

      !Exponential growth phase at passage 3
      ELSE IF (TIME .LE. 192.) THEN
      alfa=p1*NS**10+p2*NS**9+p3*NS**8+p4*NS**7+p5*NS**6+p6*NS**5+&
      p7*NS**4+p8*NS**3+p9*NS**2+p10*NS**1+p11
      !alfa: cell division rate (1/h); function of cell number; NS:
      !total # of cells
      RN=N*(delta*alfa-beta-gamma1)
      !N: normal cell #; alfa is multiplied by the factor delta
```

```
      RS=N*gamma1

      !Lag phase at passage 4
      ELSE IF (TIME .LE. 233.9) THEN
      RN=0.
      RS=0.
      NS30=NS

      !Exponential growth phase at passage 4
      ELSE
      NSF=NS*4e4/NS30
      !Convert accumulated total cell # (NS) to total cell # in single
      !dish (NSF)
      alfa=p1*NSF**10+p2*NSF**9+p3*NSF**8+p4*NSF**7+p5*NSF**6+p6*NSF**5&
      +p7*NSF**4+p8*NSF**3+p9*NSF**2+p10*NSF**1+p11
      RN=N*(delta*alfa-beta-gamma2)
      RS=N*gamma2
      END IF

      N=INTEG(RN,N0)     !Integrate RN (dN/dt) with initial value N0
      S=INTEG(RS,S0)     !Integrate RS (dS/dt) with initial value S0
      NS=N+S
 END  !End of Derivative Segment

 TERMT(TIME .GE. TSTOP)

END   !End of Dynamic Segment

END   !End of program

-------------------------------------------------------------------------
!This is the command file

! File: CR5.cmd
set weditg=.false.       !suppress output from schedule
set hvdprn=.false.       !suppress hihg volume display
output /clear            !suppress output
PREPARE TIME,N,S,NS
start              !run the simulation as soon as loaded


-------------------------------------------------------------------------
%This is the m file which saved the parameters of optimization

% File: Cr5.m

% Optimization algorithm
% Values: 0 test run, 1 default, 2 Nelder-Mead, 3 GRG2
OpAlgorithm = 3

% Do not use the data set feature.
OpDataSets = []
% Experimental data
% The data values themselves.
```

```
OpExperData = [ ...
gamma]
% The names of the data matrices.
% (Used for display only.)
OpDataNames = [ ...
"gamma" ]
% The enable/disable flags for data matrices.
% (Used for display only.)
OpEnable = [ ...
1 ]'

% Model variables to fit against experimental data.
OpTargetNames = [ ...
"NS" ...
"S" ]
% Error model.  Rows correspond to variables being fit.
% First column: heteroscedasticity parameter.
% Second column: whether to vary heteroscedasticity parameter or hold it
fixed.
OpErrModel= [ ...
2 0
2 0]

% ACSL constants to be adjusted.
OpAdjustable = [ ...
"DELTA" ...
"GAMMA1" ...
"GAMMA2" ]
% Starting values of the ACSL constants.
OpStartValues = [ ...
1 0.0574 0.0574 ]

% Constraints.
% List of parameters on which there are constraints.
OpConstrained = [ ...
"DELTA" ...
"DELTA" ...
"GAMMA1" ...
"GAMMA1" ...
"GAMMA2" ...
"GAMMA2" ]
% Constraints themselves.  One constraint per row.
OpConstraints= [ ...
0 -1
1  1
0 -1
1  1
0 -1
1  1 ]

OpDescriptors = [ ]
OpExogColumns = [ ]
% Descriptor values
% Descriptor values for the enabled data matrices
```

```
OpAllExpers = []
OpExperiments = []
% Exogenous data
OpAllExogNames = []
% No exogenous data are present.
OpExogData = []

% Scripts run for each experiment.
% No special commands are run before each experiment is simulated.
OpScriptNames = []
OpAllScriptNames = []

% Whether objective function is displayed during parameter estimation.
OpVerbose=0

% Whether we run scripts at conclusion
% 0 = run no scripts, 1 = run if successful, 2 = run always
OpConcludeAct=1

% Script or scripts if any to run at conclusion.
OpConcludeScript=[ ...
"cmpplain"
"setop" ]

% End of file
```

Appendix I: Derivation of mutation rates

The mutation rate μ is modified from fluctuation analysis proposed by Luria and Delbruck {32}. The derivation of mutation rates discussed here is represented by the immortalization of normal cells. In Chapter 1, the mutation rate μ_1 is used in Equation 1.2 that

$$\frac{dI(t)}{dt} = I(t)\cdot[\alpha_2(t) - \beta_2(t)] + \mu_1(t)\cdot\alpha_1(t)\cdot N(t) \qquad (1.2)$$

where I and N are the number of immortal and normal cells, respectively, α_2 and β_2 are the division and death rates of immortal cells, α_1 is the division rate of normal cells, and μ_1 represents the probability of mutation that a normal cell divides into one normal cell and one immortal cell, *i.e.* the number of mutation per cell division. In contrast, the mutation rate obtained from fluctuation analysis (v) is defined as the mutations per cell per division cycle and calculated as

$$v = \frac{(\ln 2)(-\ln P_0)}{N_f - N_0} \qquad (6.1)$$

where P_0 represents the fraction of culture with no mutants, N_f and N_0 are the final and initial number of cell {32}.

To modified v for the modeling purpose, the relation between the unit "division cycle" , denoted as τ, and time unit "t" is defined as

$$\tau = \frac{\alpha_1}{\ln 2}\cdot t \qquad (I.1)$$

When t=0, τ is equal to 0. When t=(ln 2)/α_1, *i.e.* potential doubling time, τ is equal to 1 at which cells complete one division cycle. Since it is assumed that mutation only occurs at cell division, potential doubling time is counted as cell cycle time which ignores the impact of cell death.

With division cycle defined as above, the number of immortal cells mutated from normal cells (I_m) during time interval *dt* is calculated as

$$dI_m = \nu \cdot N \cdot d\tau$$
$$= \nu \cdot N \cdot (\frac{\alpha_1}{\ln 2} \cdot dt) \qquad \text{(I.2)}$$

where α_1 is assumed to be constant. This assumption is true from passage to passage, since the cell division rates are very consistent between passages in my experiments. However, in order to fully accomplish the assumption, experimental design should be modified that cells have to be passaged before confluency is reached to reduce the impact of crowding factor on division rates α_1 within each passage.

By applying Equation 6.1 into Equation I.2, dI_m can be rewritten as

$$dI_m = \frac{-\ln P_0}{N_f - N_0} \cdot \alpha_1 \cdot N \cdot dt \qquad \text{(I.3)}$$

By comparing Equation I.3 to Equation 1.2, the mutation rate μ_1 in the model can be calculated as

$$\mu_1 = \frac{-\ln P_0}{N_f - N_0} \qquad \text{(I.4)}$$